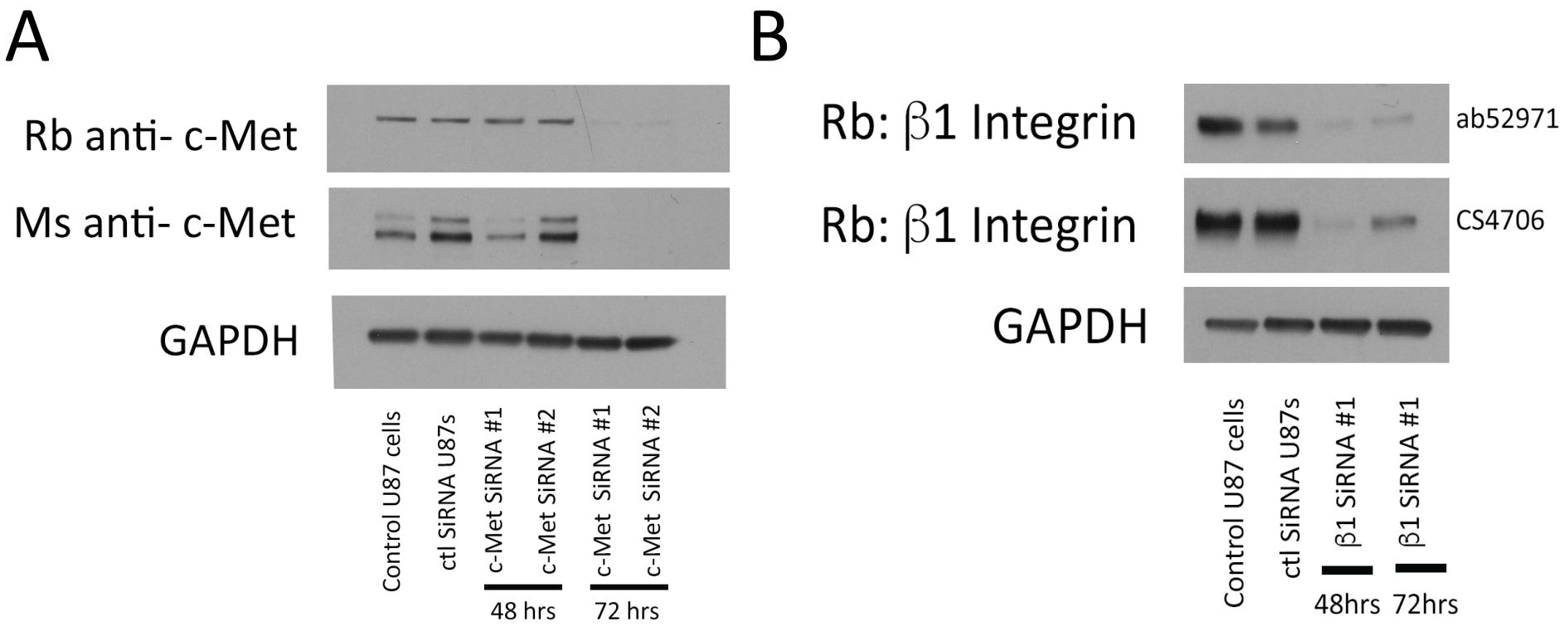

Fig. S1. Validation of antibodies used with siRNA. Related to **Figs. 1-8**. (A) Western blot of U87 cells that were untransfected (first lane), transfected with siRNA targeting control sequences (second lane), and transfected with siRNA targeting two different sequences in human c-Met and analyzed 48 (lanes three and four) and 72 (lanes five and six) hours later. Blotting was done to verify two different c-Met antibodies: rabbit ab51067 and mouse cst3148. (**B**) Western blot of U87 cells that were untransfected (first lane), transfected with siRNA targeting control sequences (second lane), and transfected with siRNA targeting human β1 integrin and analyzed 48 (lane three) and 72 (lane four) hours later. Blotting was done to verify two different rabbit anti-human β1 integrin antibodies: ab52971 and CS4706.

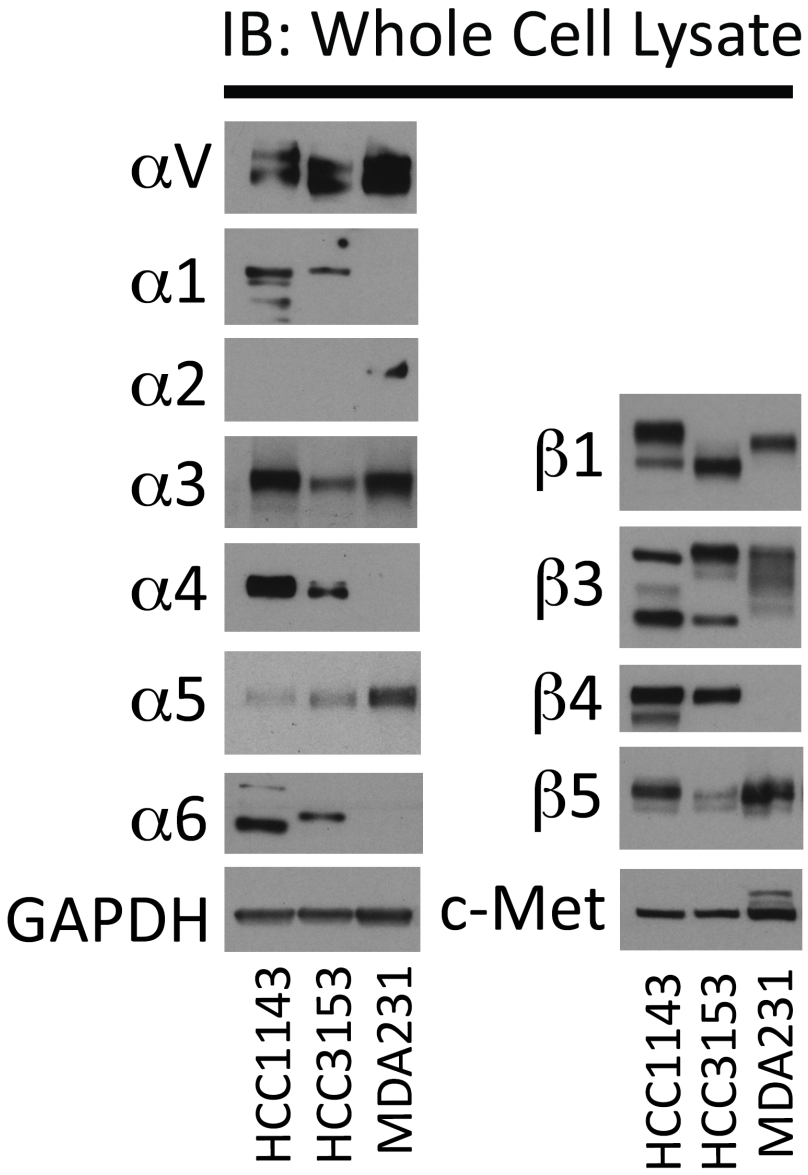

Fig. S2. Western blot of integrin and c-Met expression in 3 different breast cancer cell lines. Related to **Fig. 1*A***. Western blotting of HCC1143, HCC3153, and MDA-MB-231 breast cancer cells was performed for 7 α integrins, 4 β integrins, and c-Met.

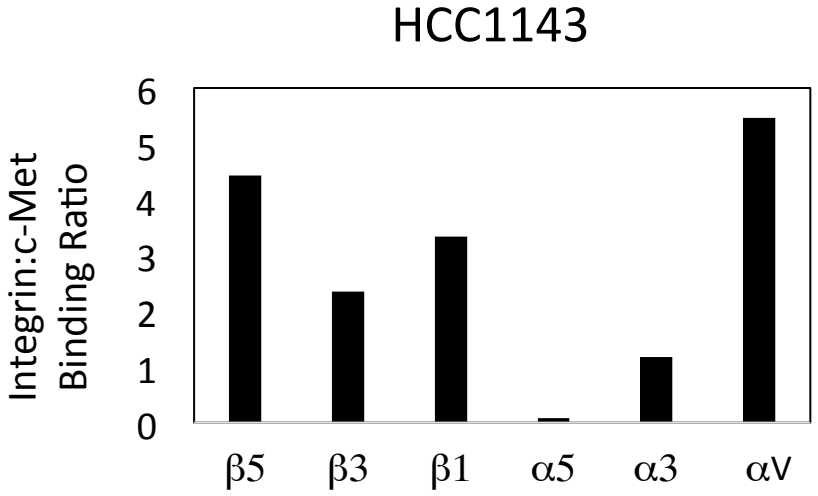

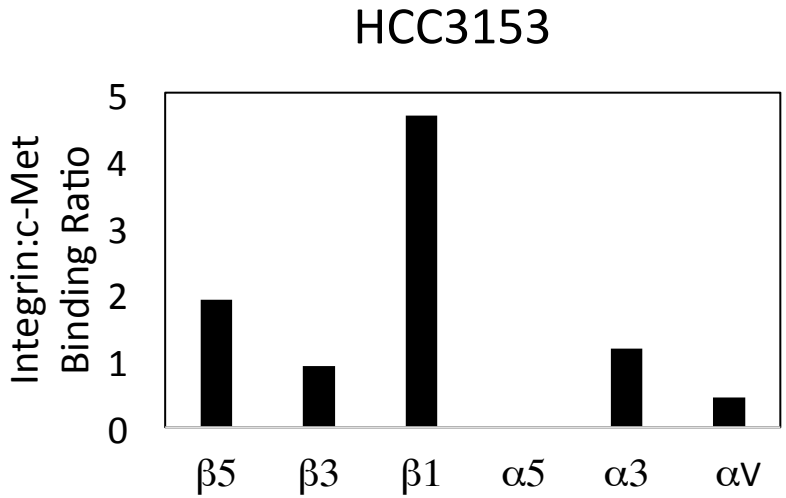

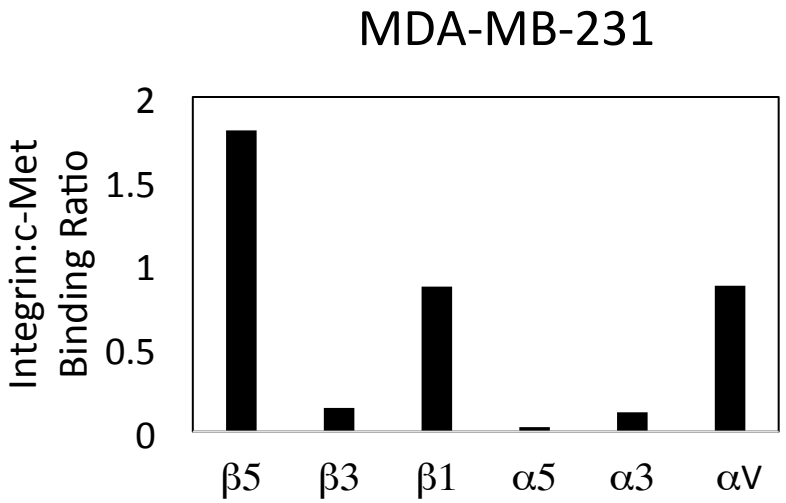

Fig. S3. Quantification of six different integrin:c-Met binding ratios in three different breast cancer cell lines. Related to **Fig. 1*A***. The c-Met IPs performed in Fig. 1A were quantified with the ratio of densitometry of six different integrins to the c-Met densitometery calculated as integrin:c-Met binding ratios, with higher ratios suggesting more binding. Of the six integrins, four were deemed to bind c-Met significantly in HCC1143, two in HCC3153, and three in MDA-MB-231, with β1 and β5 integrin the only two to bind strongly in all three cell lines. The former was chosen for further investigation based on greater supportive evidence for its role in cancer metastases.

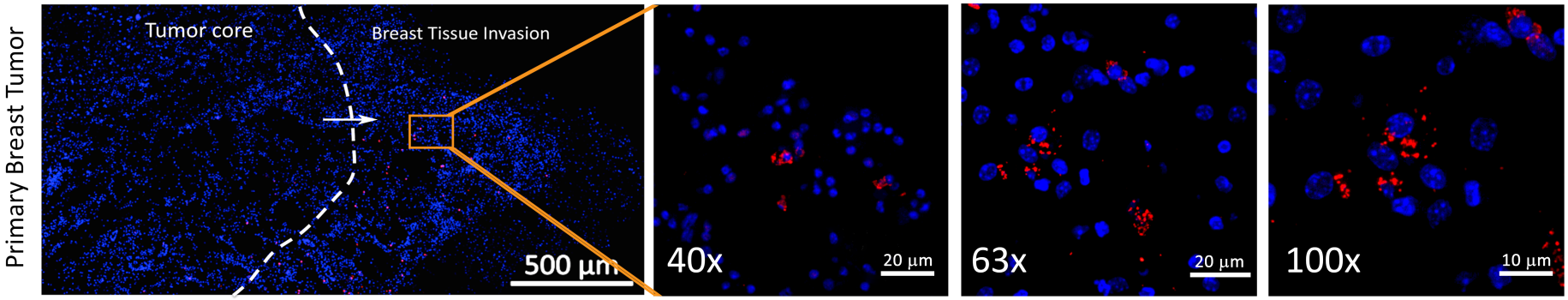

Fig. S4. A second example of PLA for c-Met/β1 complex detection in a primary MDA-MB-231 mammary pad xenograft. Related to **Fig. 1*B***. After MDA-MB-231 breast cancer cells were implanted in the mammary pads of immunodeficient mice, PLA revealed c-Met/β1 integrin complex formation at the invasive edge of these xenografts. One representative tumor is shown in **Fig. 1*B*** and another representative tumor is shown here.

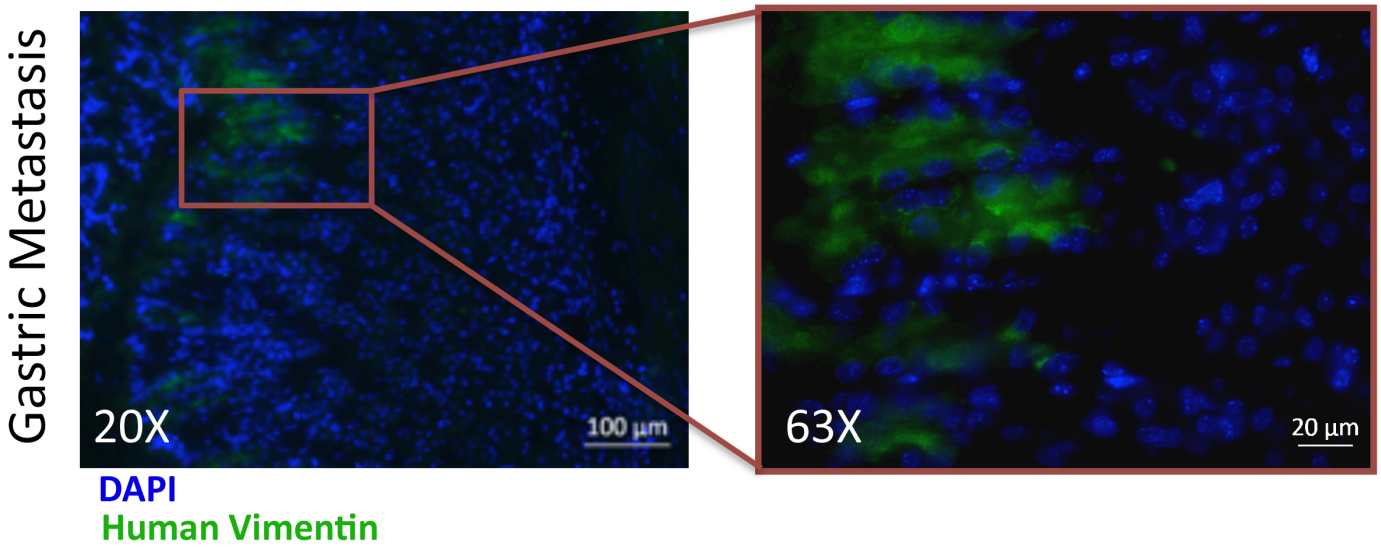

Fig. S5. Vimentin staining reveals a gastric metastasis from MDA-MB-231 implanted in mammary pads of immunodeficient mice. Related to **Fig. 1*C***. After MDA-MB-231 breast cancer cells were implanted in the mammary pads of immunodeficient mice, one mouse developed a gastric metastasis as confirmed here by human vimentin (green) staining revealing the metastasis. PLA of this metastasis as shown in **Fig. 1*C*** and quantified in **Fig. 1*D*** revealed increased c-Met/β1 integrin complex formation in the metastasis relative to the primary tumor in the mammary pad.

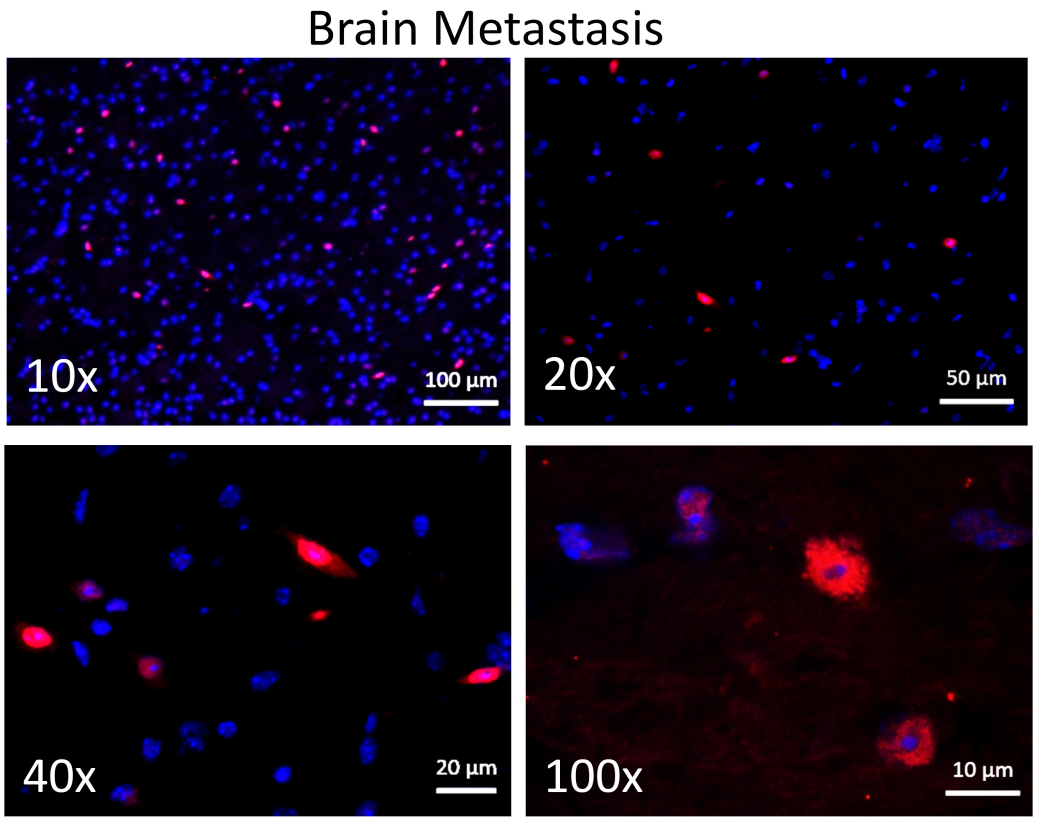

Fig. S6. Additional PLA images of brain metastasis from MDA-MB-231 xenografts implanted in mammary pads. Related to **Fig. 1*C***. After MDA-MB-231 breast cancer cells were implanted in the mammary pads of immunodeficient mice, one mouse developed a brain metastasis. PLA of this metastasis as shown in **Fig. 1*C*** and quantified in **Fig. 1*D*** revealed increased c-Met/β1 integrin complex formation in the metastasis relative to the primary tumor in the mammary pad. The 10x and 40x images of the PLA of this metastasis are shown in **Fig. 1*C***, additional 20x and 100x images are added here.

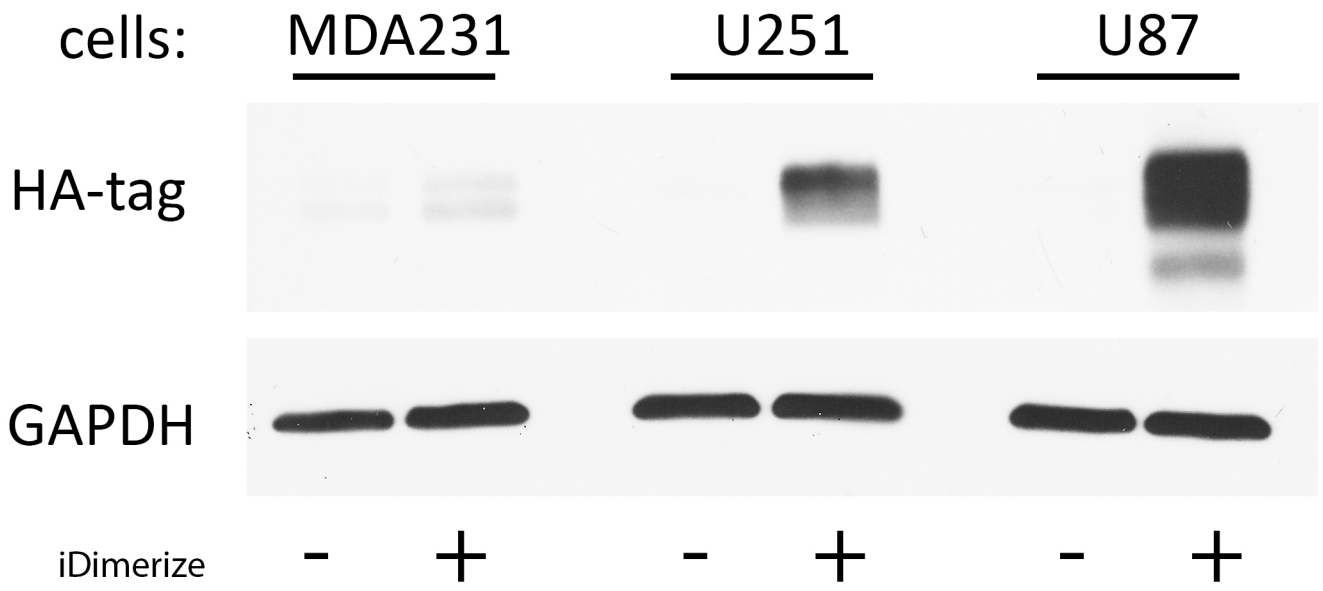

Fig. S7. Engineered expression of inducible heterodimerization system. Related to **Figs. 2, S7-S11, and S19-S23**. Western blot from MDA-MB-231, U251, and U87 cells engineered to express β1 integrin and c-Met fused to FRB (DmrC) and FKBP (DmrA) confirmed expression of the HA-tag fused to β1 integrin in all 3 cell lines transduced to express the inducible heterodimerizer system.

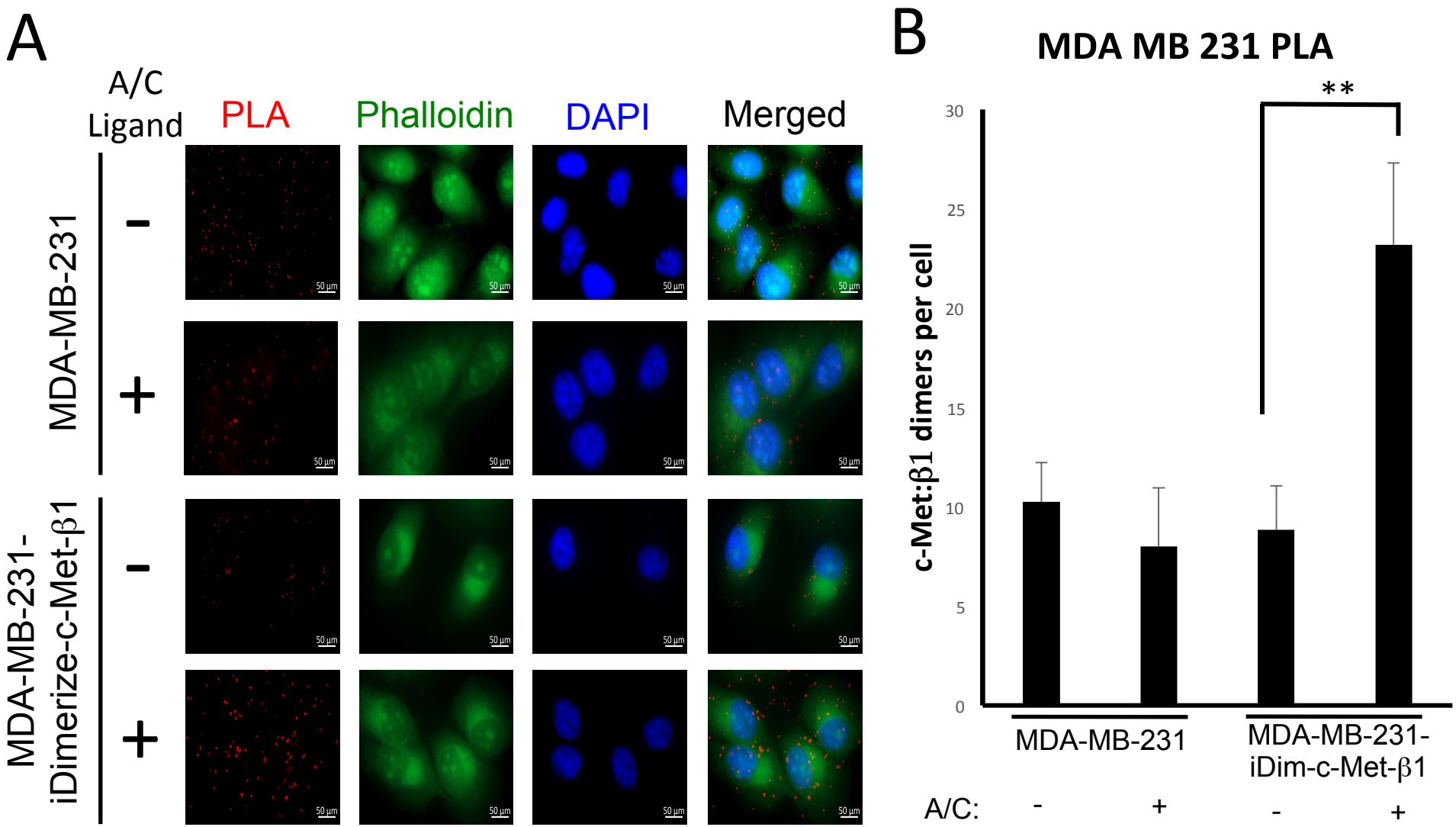

Fig. S8. Use of PLA in cultured breast cancer cells to verify inducible heterodimerization system. Related to **Fig. 2**. MDA-MB-231 and MDA-MB-231-iDimerize-c-Met-β1 cells were treated without or with the A/C ligand for 12 hours on chamber slides, after which PLAs were performed to assess c-Met/β1 complex formation. A/C ligand increased the presence of PLA red dots in MDA-MB-231-iDimerize-c-Met-β1 cells relative to the background seen in MDA-MB-231-iDimerize-c-Met-β1 cells without A/C ligand (*P*=0.002), with MDA-MB-231 cells with or without A/C ligand at the same background as MDA-MB-231 cells without A/C ligand (*P*=0.2). 100x magnification, scale bars 50 μm. * *P*<0.05; ** *P*<0.01 *** *P*<0.001.

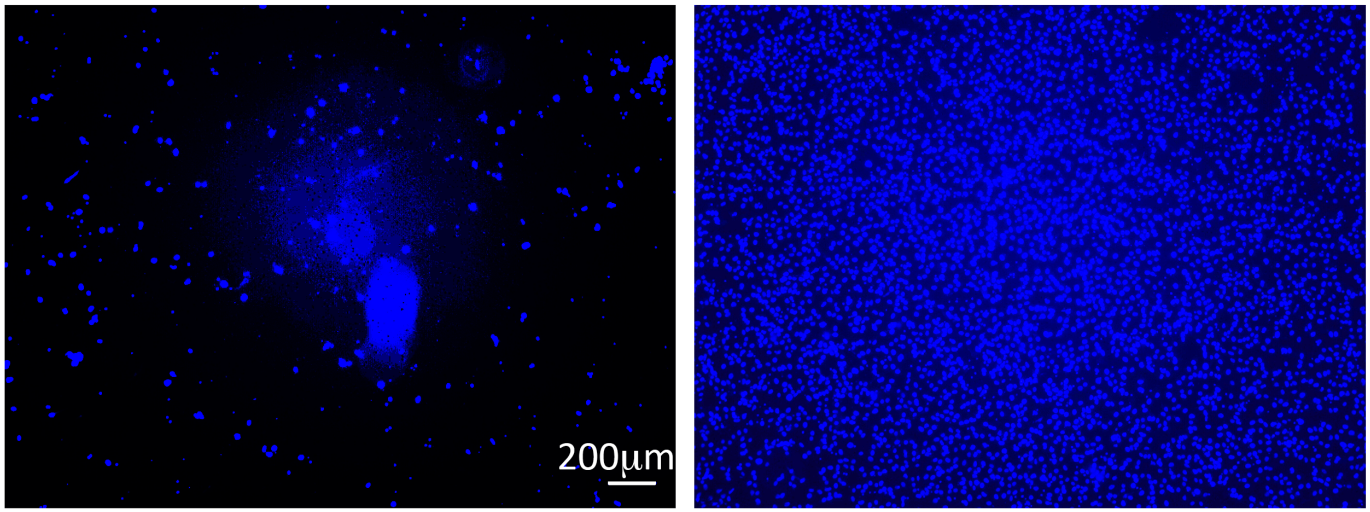

Fig. S9. Matrigel images from MDA-MB-231-iDimerize-c-Met-β1 cells. Related to **Fig. 2*E***. MDA-MB-231-iDimerize-c-Met-β1 cells were treated with AP21967 or vehicle (control), followed by matrigel invasion assays. AP21967 increased MDA-MB-231-iDimerize-c-Met-β1 cell invasion in matrigel, as quantified in **Fig. 2*E*** (n=6/group; *P*=0.007), with representative images from the assays shown here.

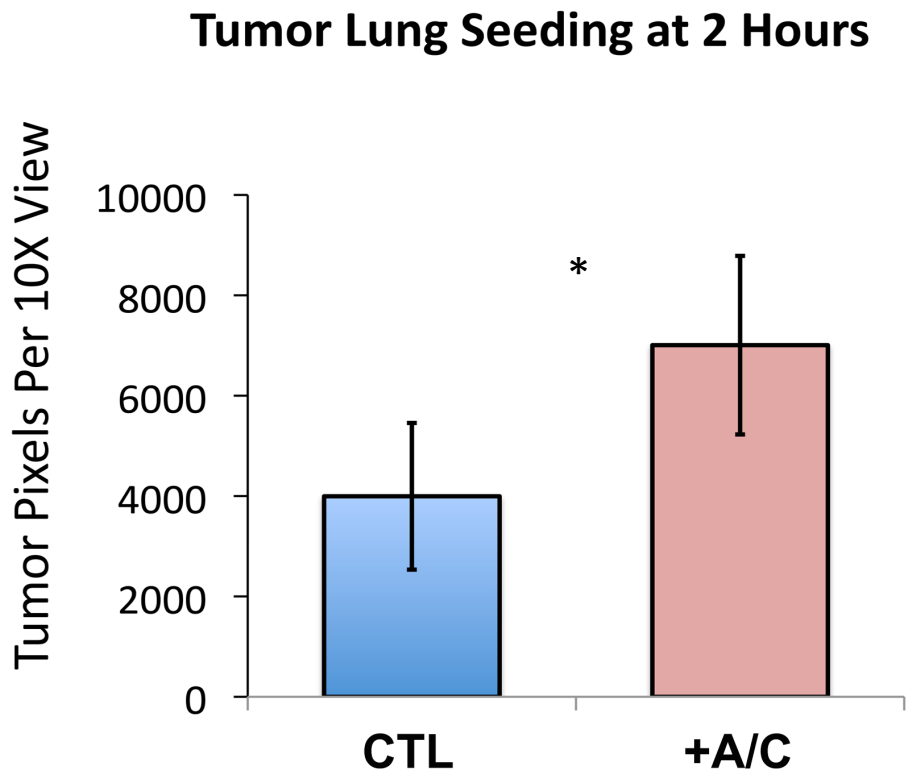

Fig. S10. Quantification of lung tumor uptake by IHC assessed two hours after tail vein injection of MDA-MB-231-iDimerize-c-Met-β1 cells pre-treated with or without A/C ligand. Related to **Fig. 2*F***. MDA-MB-231-iDimerize-c-Met-β1 cells were pre-treated for two hours with or without AP21967, followed by tail vein injection into NSG mice (n=6 mice/group). After two hours, mice receiving AP21967-pretreated cells exhibited more human vimentin staining by IHC vs. those pre-treated with vehicle, as shown in images in **Fig. 2*F*** and quantified here (*P*=0.02). * *P*<0.05; ** *P*<0.01 *** *P*<0.001.

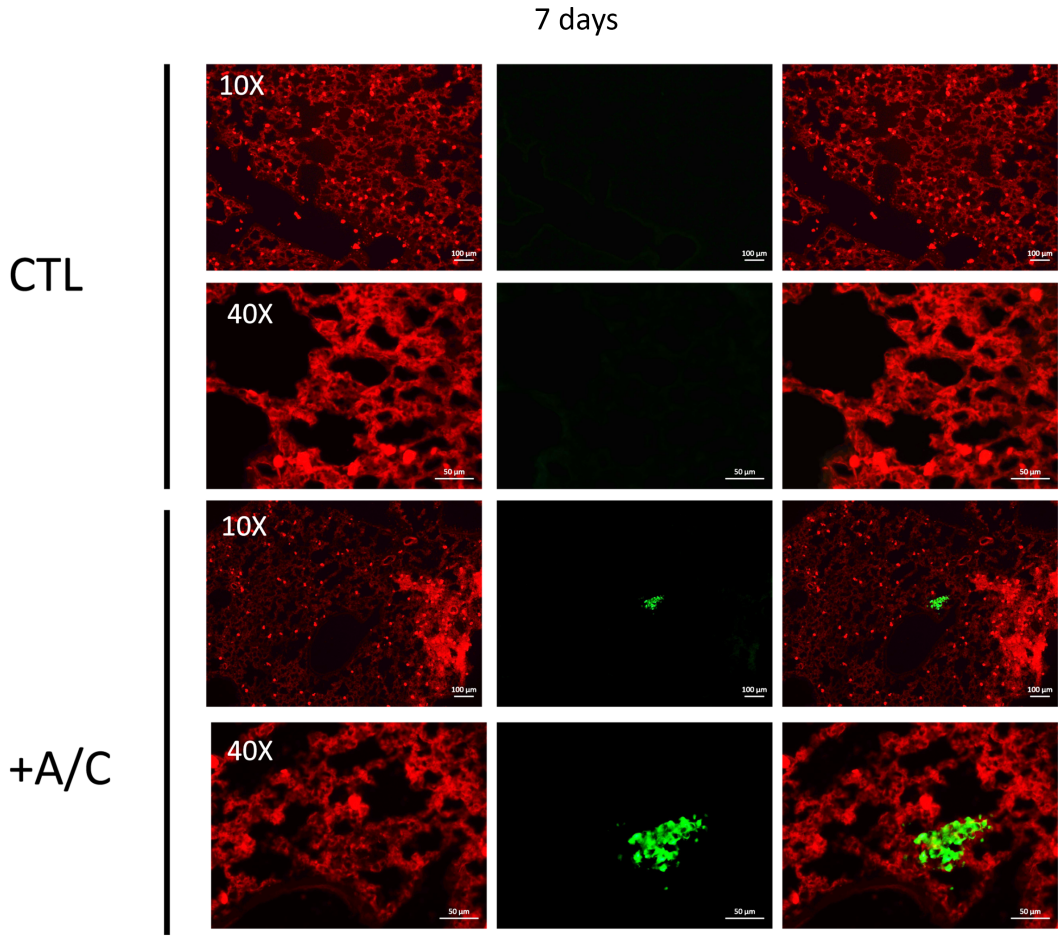

Fig. S11. Additional images of lung tumor uptake by IHC assessed seven days after tail vein injection of MDA-MB-231-iDimerize-c-Met-β1 cells pre-treated with or without A/C ligand. Related to **Fig. 2*G***. MDA-MB-231-iDimerize-c-Met-β1 cells were pre-treated for two hours with or without AP21967, followed by tail vein injection into NSG mice (n=6 mice/group). After seven days, there were foci of nodular human vimentin staining after tail vein injection of cells pre-treated with AP21967 compared to no staining when injecting vehicle pre-treated cells (lack of staining in control group prevented statistical comparison). **Fig. 2*G*** shows 40x magnification. Here we show 10x magnification alongside 40x.

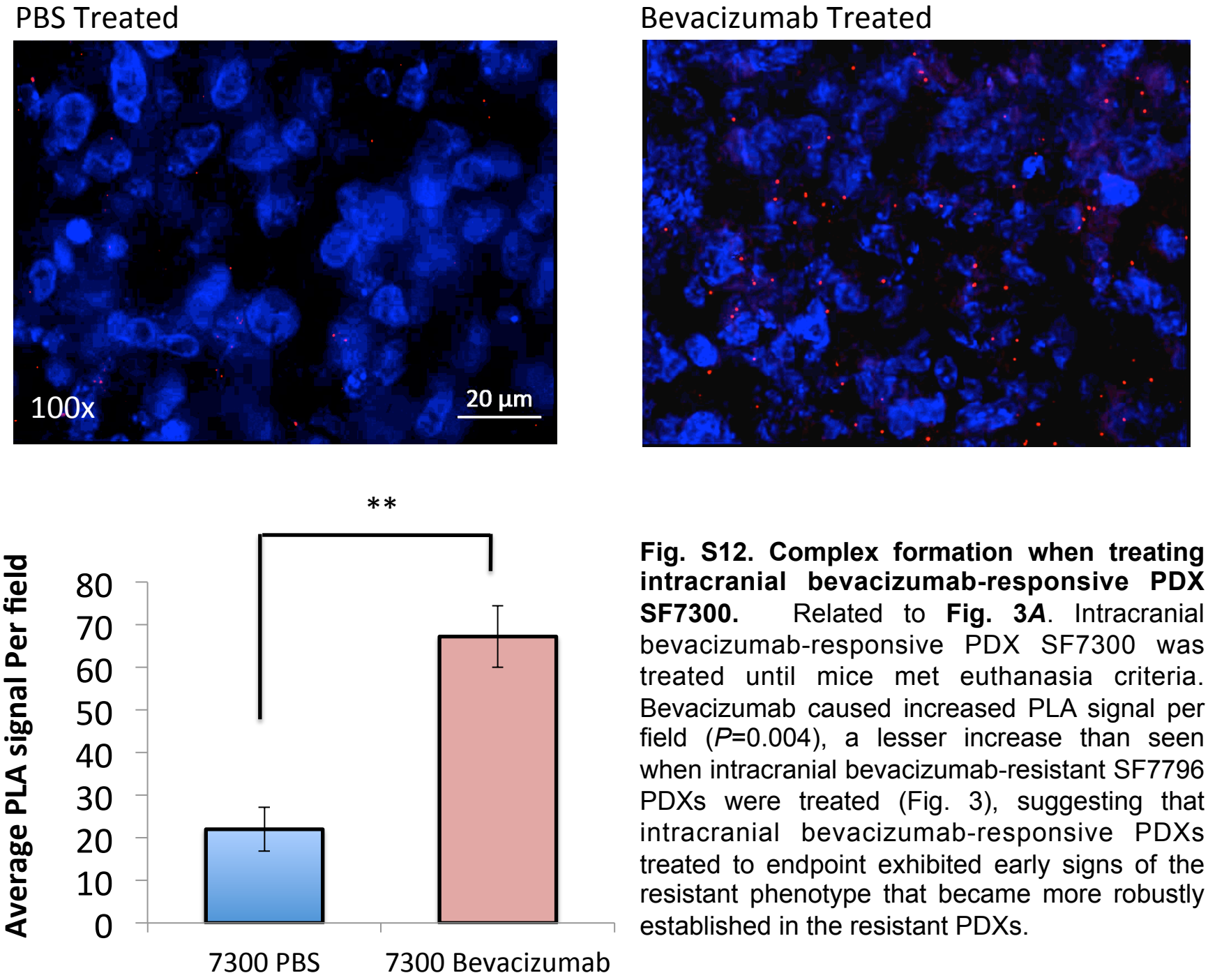

Fig. S12. Complex formation when treating intracranial bevacizumab-responsive PDX SF7300. Related to **Fig. 3*A***. Intracranial bevacizumab-responsive PDX SF7300 was treated until mice met euthanasia criteria. Bevacizumab caused increased PLA signal per field (*P*=0.004), a lesser increase than seen when intracranial bevacizumab-resistant SF7796 PDXs were treated (Fig. 3), suggesting that intracranial bevacizumab-responsive PDXs treated to endpoint exhibited early signs of the resistant phenotype that became more robustly established in the resistant PDXs.

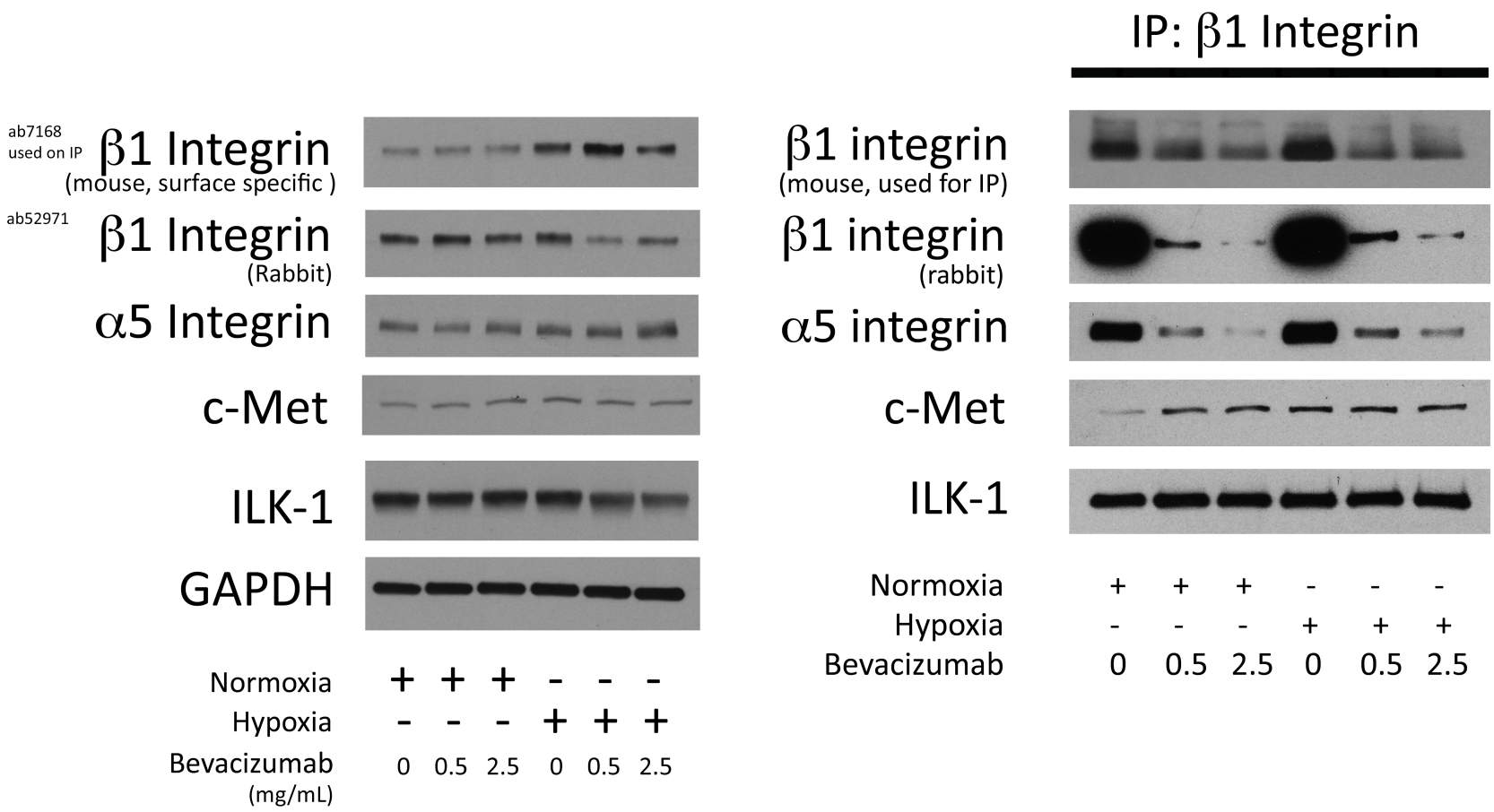

Fig. S13. Western blots on whole cell lysates and immunoprecipitates of cultured GBM cells treated with bevacizumab in normoxia vs. hypoxia. Related to **Fig. 3*D***. U87 cells were treated in hypoxia (1% oxygen) or with bevacizumab (0.5 or 2.5 mg/mL) for 48 hours. Shown to the left are the western blots from whole cell lysates, while shown to the right are the blots from β1 integrin immunoprecipitates generated using mouse ab7168. Interestingly, bevacizumab reduced the ability of rabbit ab52971 to recognize β1 integrin in the immunoprecipitates, but β1 integrin levels did not change in response to bevacizumab based on the other blots.

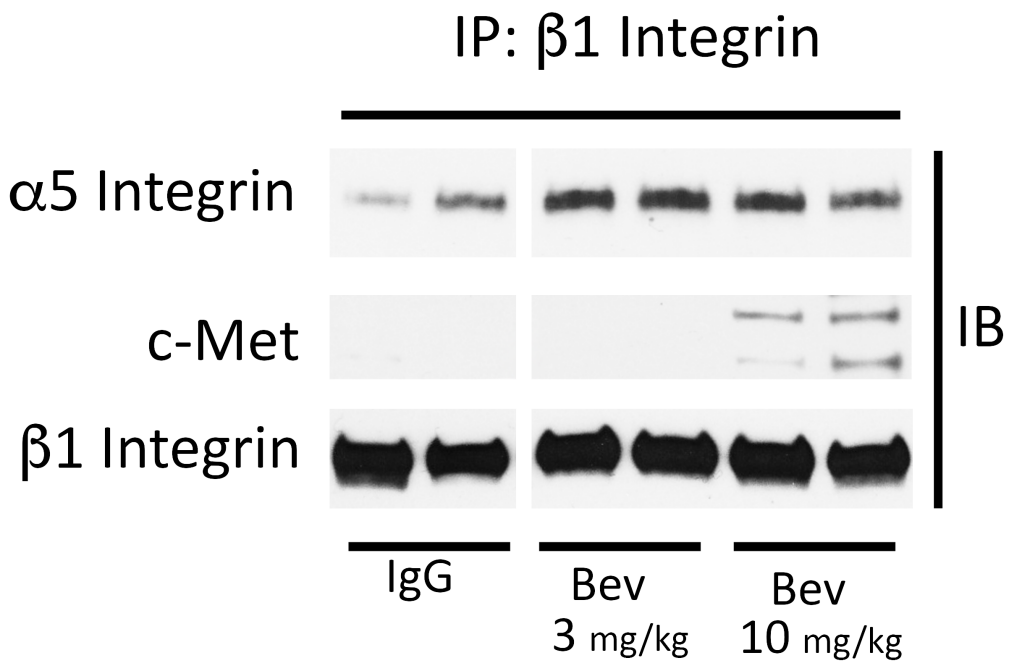

Fig. S14. Western blots on whole cell lysates and immunoprecipitates of cultured GBM cells treated with bevacizumab in normoxia vs. hypoxia. Related to **Fig. 3**. Subcutaneous U87 xenografts were treated with IgG and bevacizumab at 3 and 10 mg/kg, with tumor lysate IP revealing dose-dependent c-Met/β1 integrin binding.

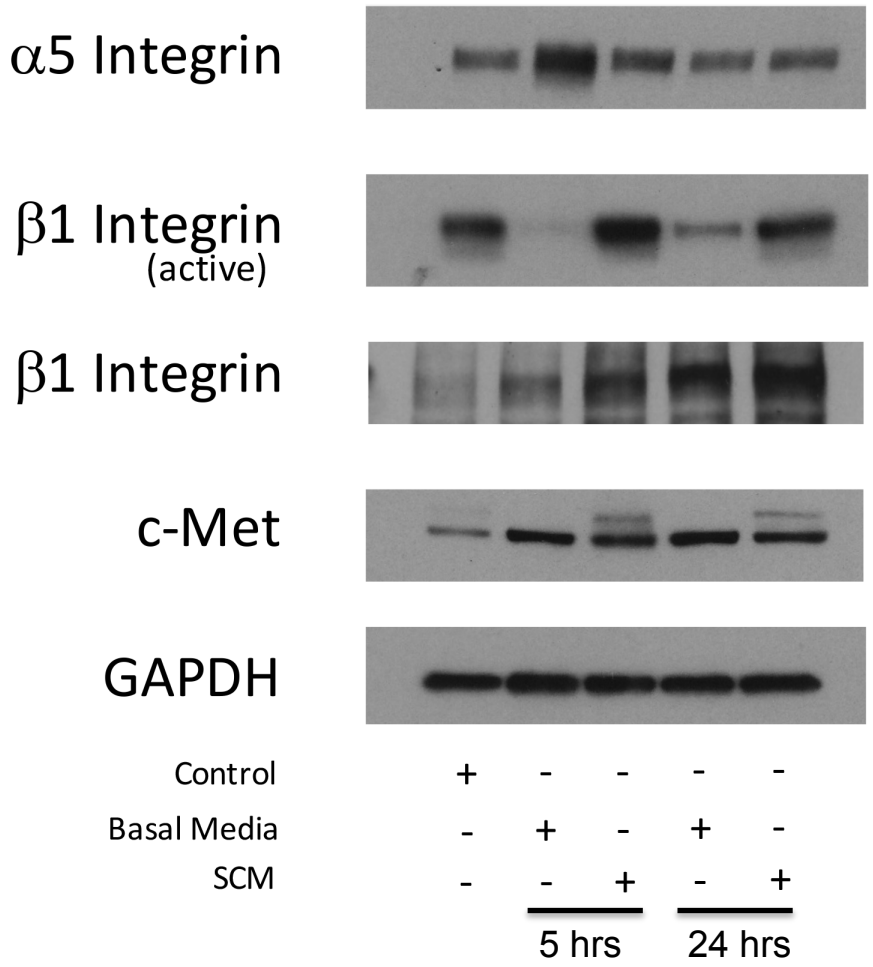

Fig. S15. Western blots on whole cell lysates of cultured GBM cells treated with endothelial cell conditioned media. Related to **Fig. 4*A***. U87 cells were grown in basal HUVEC media or HUVEC serum conditioned media (SCM) for 5 or 24 hours, after which the whole cell lysates underwent western blotting for the antigens shown here.

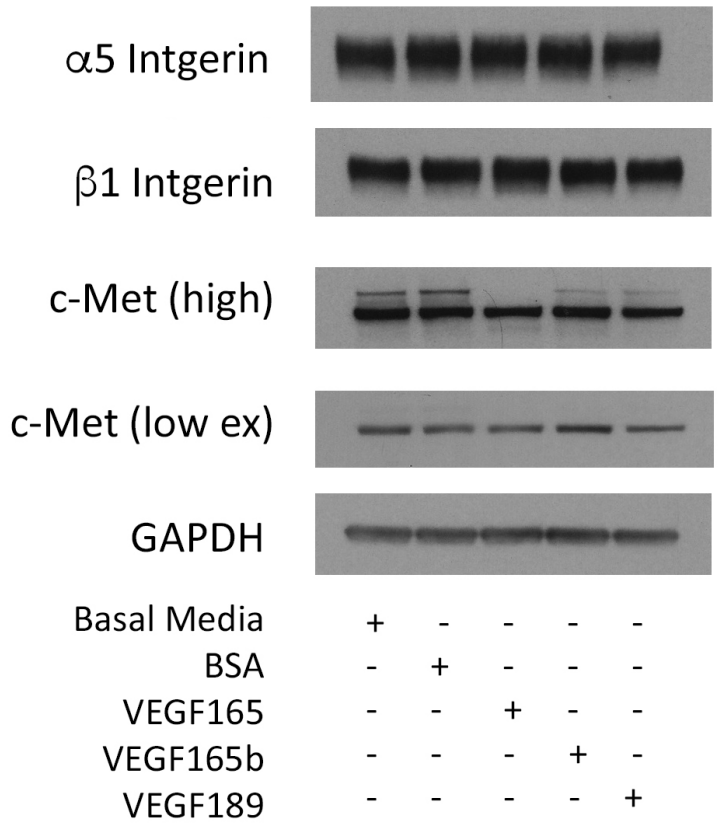

Fig. S16. Western blots on whole cell lysates of cultured GBM cells treated with various VEGF isoforms. Related to **Fig. 4*B***. U87 cells were incubated with basal media or 100 ng/mL BSA, VEGF165, VEGF165b, or VEGF189 for 2 hours, as shown in **Fig. 4*B***, after which western blots were performed on the whole cell lysates for the antigens shown here.

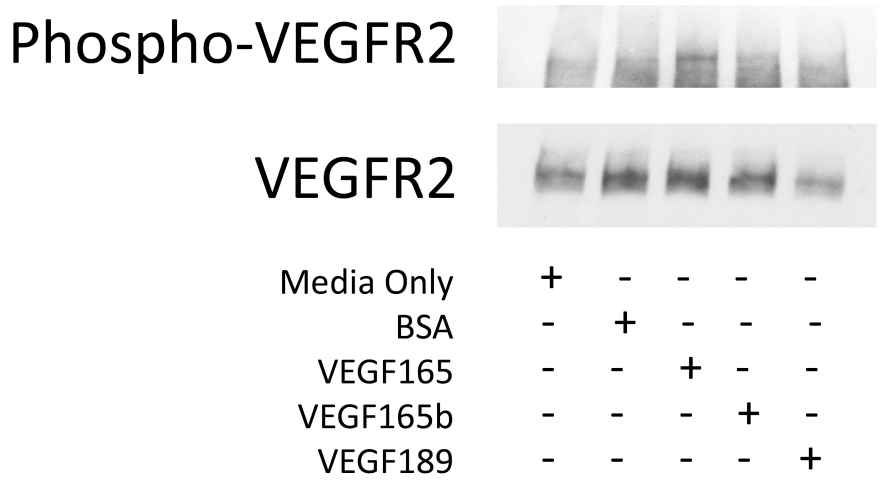

Fig. S17. VEGF165 induces VEGFR2 phosphorylation more than VEGF165b or VEGF189 in cultured GBM cells. Related to **Fig. 4*B***. U87 cells were incubated with basal media or 100 ng/mL BSA, VEGF165, VEGF165b, or VEGF189 for 2 hours, as shown in **Fig. 4*B***, with levels of phosphorylated and total VEGR2 assessed by western blot.

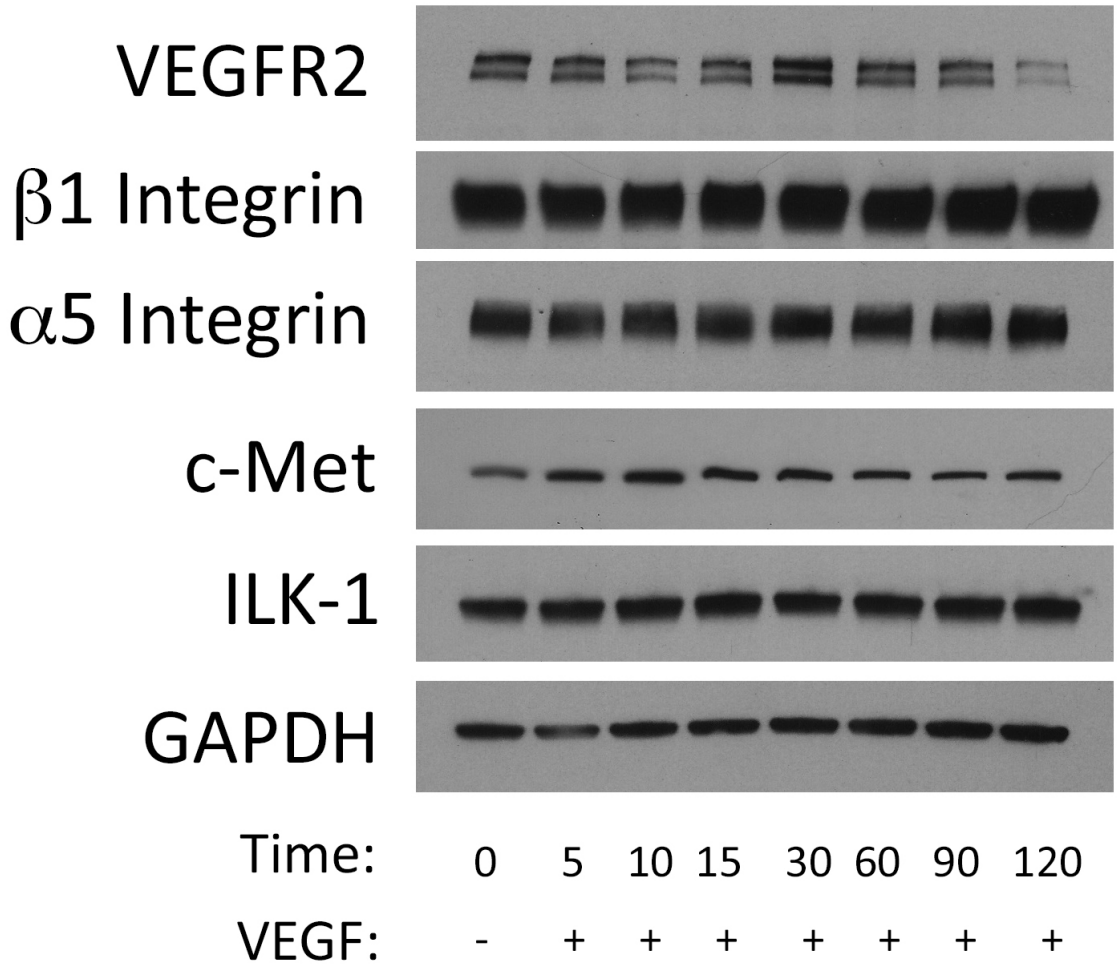

Fig. S18. Western blots on whole cell lysates of cultured GBM cells treated with endothelial cell conditioned media or various VEGF isoforms. Related to **Figs. 4*C-D***. U87 cells were treated with VEGF165 for variable time points shown here in minutes, as described in **Figs. 4*C-D***. Western blots for the antigens listed here were then performed on the resulting whole cell lysates.

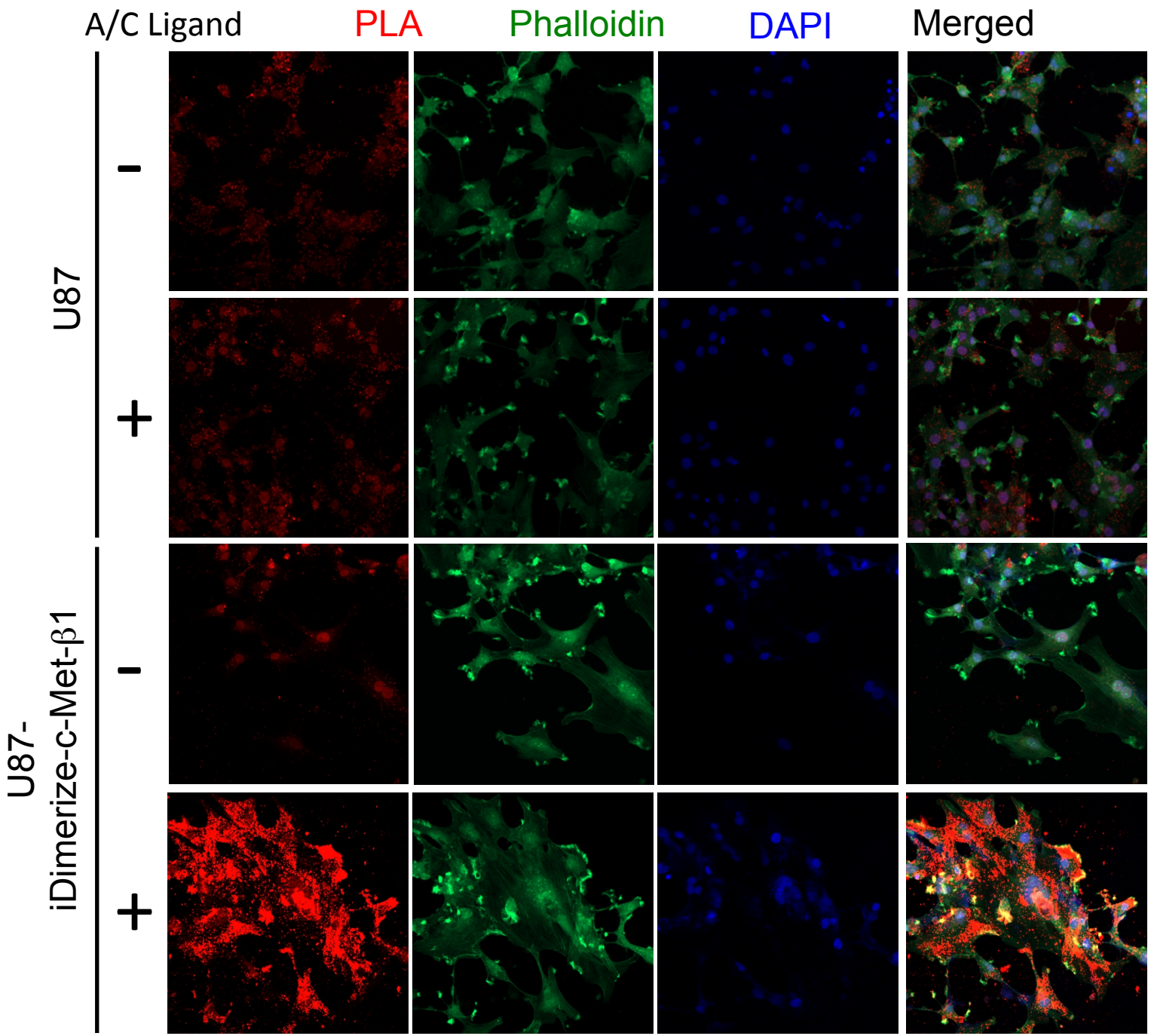

Fig. S19. Induction of c-Met/β1 integrin binding assessed by PLA in GBM cells. U87 cells without or with inducible heterodimerization were plated on chamber slides and treated with or without A/C ligand for 12 hours, after which PLA was performed to measure c-Met/β1 integrin complex formation. At the same exposure used in **Fig. S8**, the more robust expression of the inducible heterodimerization system in U87 cells compared to MDA-MB- 231 cells led to saturated red staining requiring lower exposure to quantify (**Fig. S20**). 100x, scale bars 50 μm.

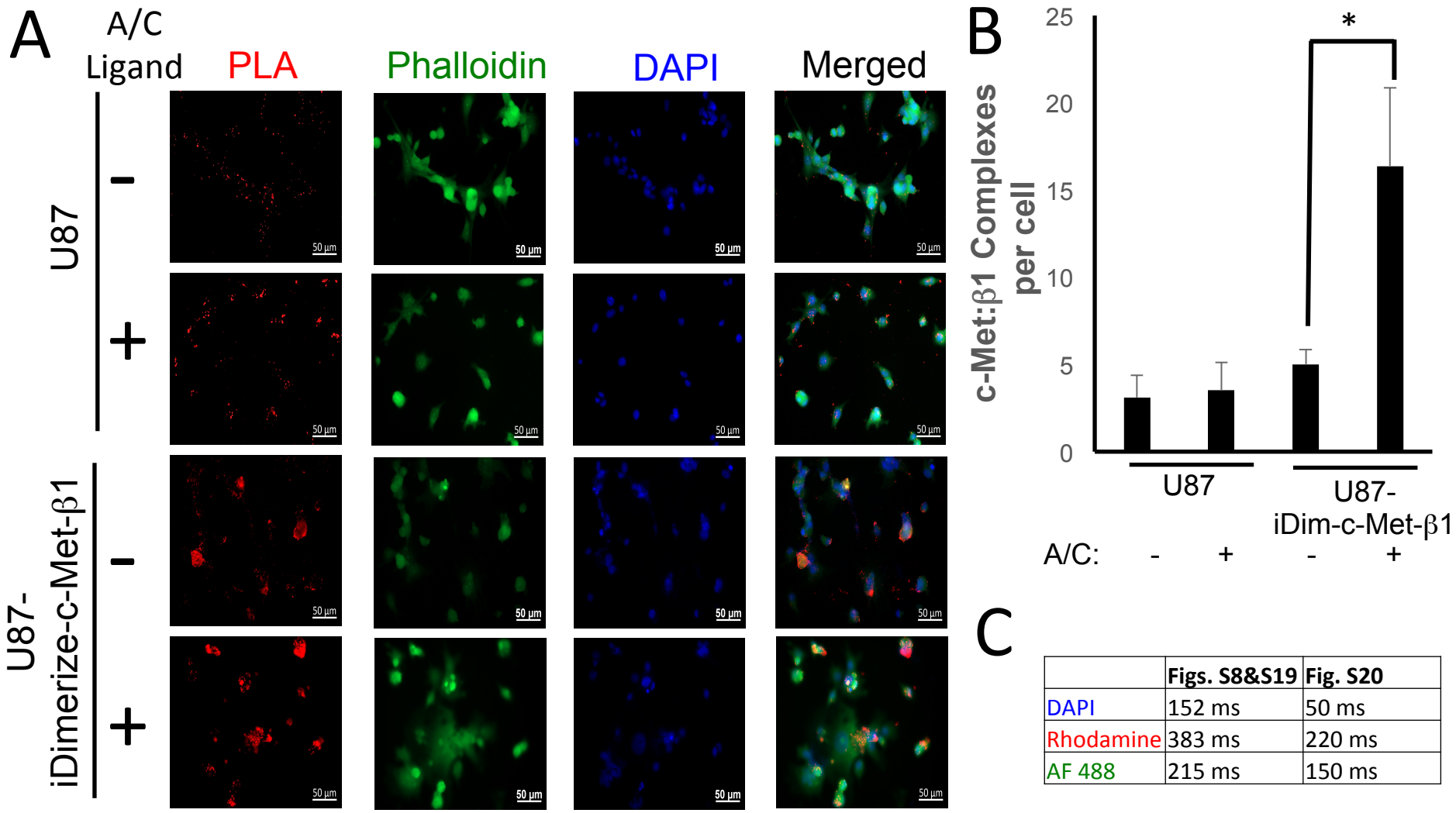

C

	Figs. S8&S19	Fig. S20
DAPI	152 ms	50 ms
Rhodamine	383 ms	220 ms
AF 488	215 ms	150 ms

Fig. S20. Induction of c-Met/β1 integrin binding assessed by PLA in GBM cells. (A) U87 cells without or with inducible heterodimerization were plated on chamber slides and treated with or without A/C ligand for 12 hours, after which PLA was performed to measure c-Met/β1 integrin complex formation. Using a lower exposure than used in **Figs. S8 and S19** due to the more robust expression of the inducible heterodimerization system in U87 cells compared to MDA-MB- 231 cells, the red PLA staining could be visualized. (**B**) Quantification of PLA signals per cell revealed a robust increase when A/C was added to U87-iDimerize-c-Met-b1 (P=0.01), with no increase occurring when A/C was added to U87 (P=0.7). (**C**) Specific exposure times by channel used in **Figs. S8 and S19** versus **S20**. 100x magnification, scale bars 50 μm. * *P*<0.05; ** *P*<0.01 *** *P*<0.001.

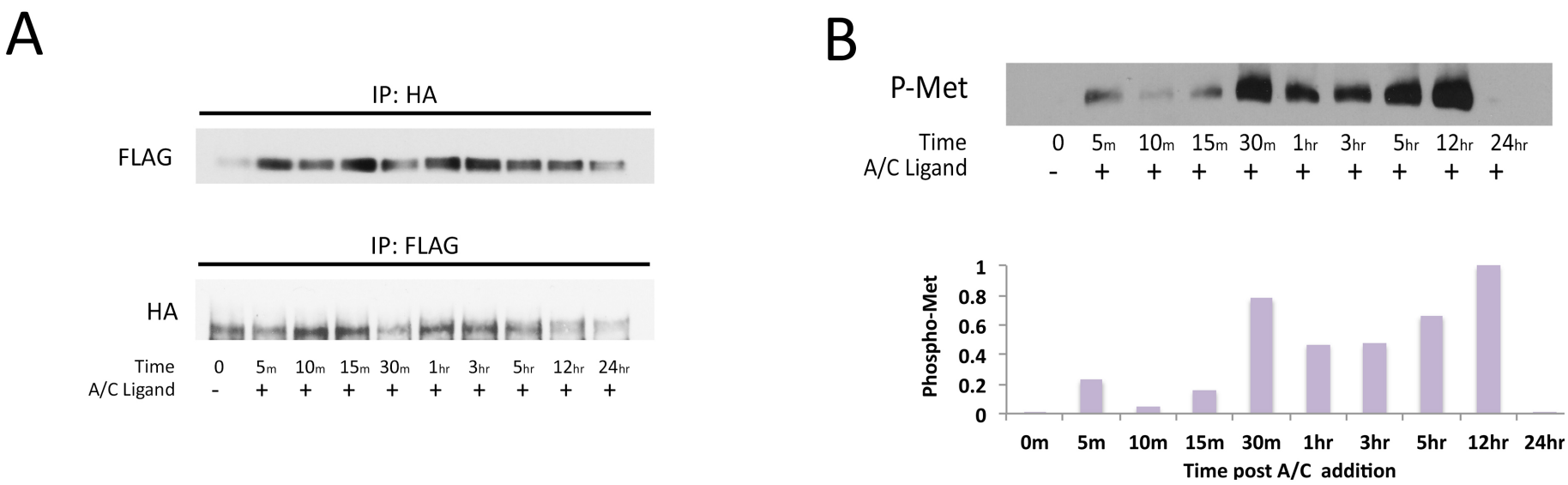

Fig. S21. Inducing c-Met/β1 integrin binding in GBM cells. (*A*) U87 and U251 GBM cells were engineered to express HA-tagged β1 integrin and FLAG-tagged c-Met fused to FRB (DmrC) and FKBP (DmrA) respectively. Engineered U87 cells were then treated with AP21967 or vehicle, after which HA and FLAG IP were used to confirm that AP21967 induced c-Met/β1 integrin binding. (***B***) Western blot was used to show increased c-Met phoshorylation after inducing c-Met/b1 integrin binding by treating U87-iDimerize-c-Met-β1 cells with AP21967.

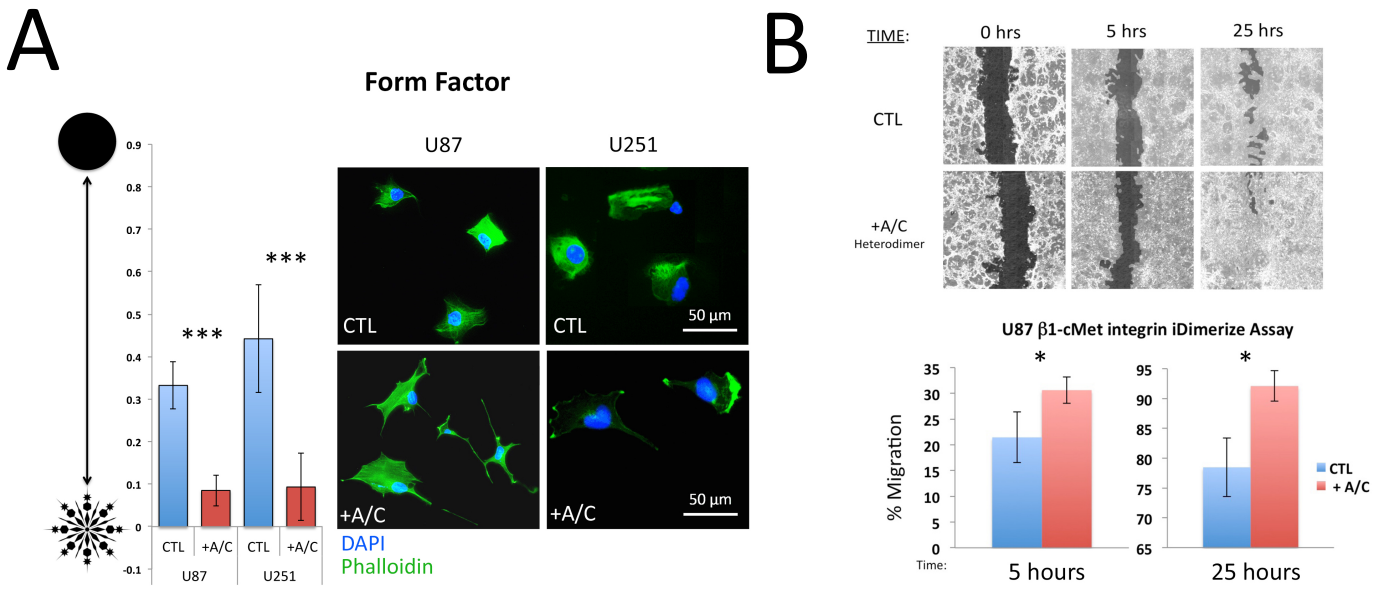

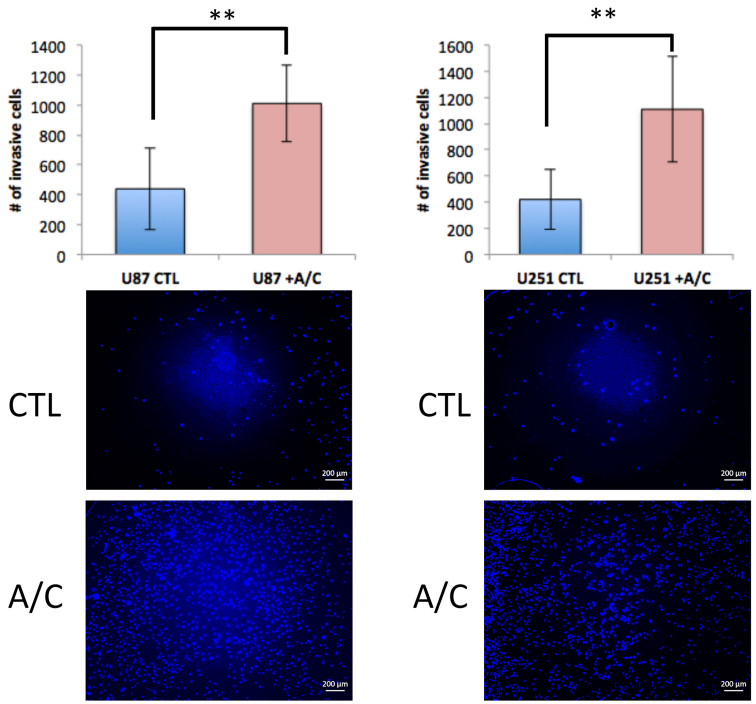

Fig. S22. Inducing c-Met/β1 integrin binding in GBM cells decreases circularity shape factor, increases tumor cell motility, and increases tumor cell invasion and adaptation to hypoxia and nutrient deprivation. (*A*) U87 and U251 cells with inducible dimerization were assessed for morphology via a Form Factor plugin on ImageJ, which revealed that AP21967 decreased circularity shape factor in both (P=1.6 X10^{-6}–2.1X10^{-7}). (***B***) U87-iDimerize-c-Met-β1 cells were scratched, and assessed after 5 and 25 hours via mosaic imaging and analyzed using the T-Scratch software to confirm that AP21967 induced migration (P=0.006 at 5 and 25 hours; n=6/group). (***C***) AP21967 also increased invasion of U87 (P=0.004) and U251 (P=0.007) cells with inducible dimerization in matrigel chambers (n=6/group). * P<0.05; ** P<0.01 *** P<0.001.

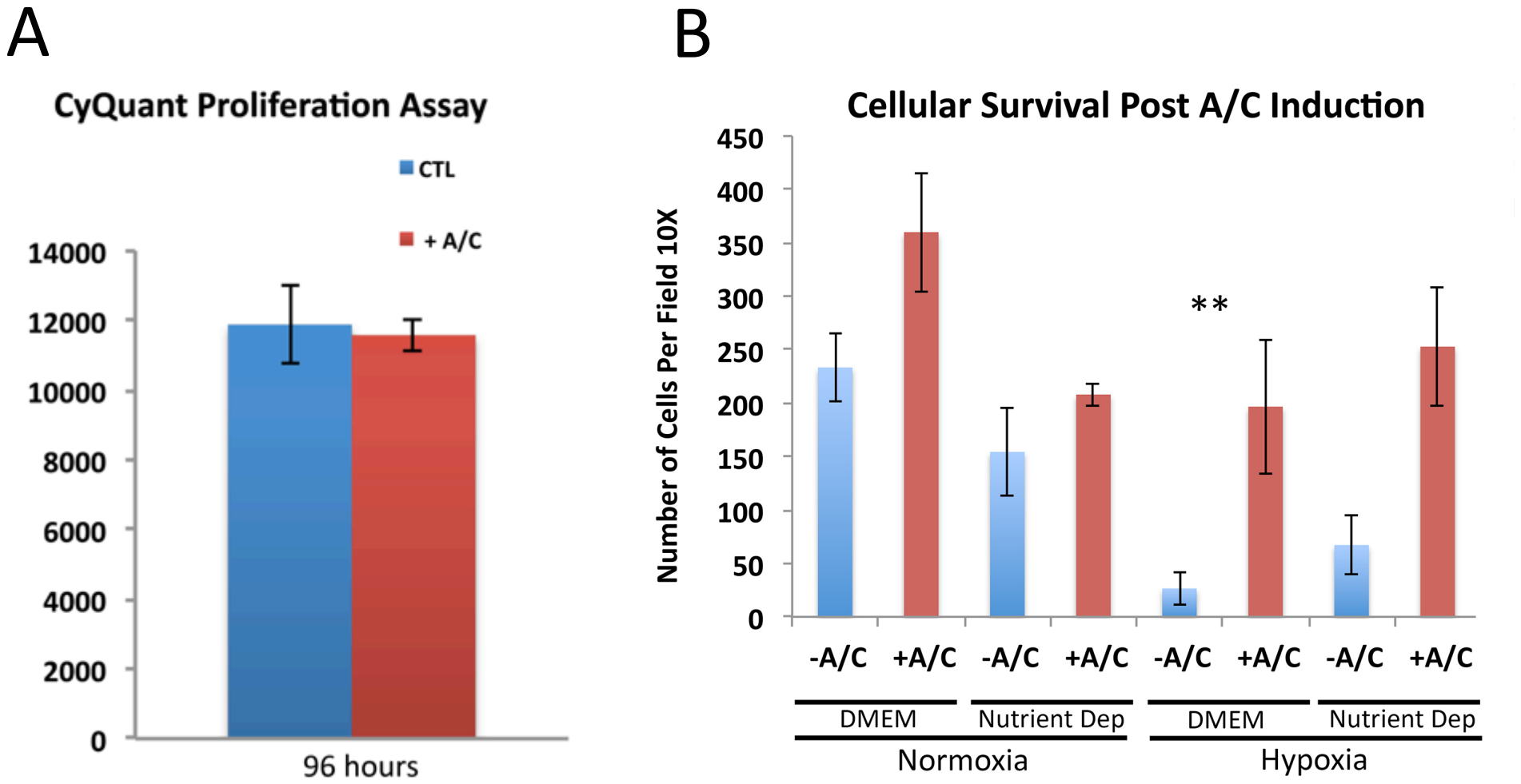

Fig. S23. Inducing c-Met/β1 integrin binding does not alter tumor cell proliferation, and increases adaptation to hypoxia and nutrient deprivation. (***A***) U87 cells with inducible heterodimerization were allowed to proliferate up to 96 hours, and assessed via CyQuant proliferation kit with no change in proliferation (*P=0.2*). (***B***) AP21967 improved survival of U87-iDimerize-c-Met-β1 cells incubated in hypoxia, with effects in nutrient (serum) deprivation not reaching significance (P=0.008 three way ANOVA for AP21967-hypoxia interaction, P=0.4 three way ANOVA for AP21967-nutrient deprivation interaction; n=3/group). * *P*<0.05; ** *P*<0.01 *** *P*<0.001.

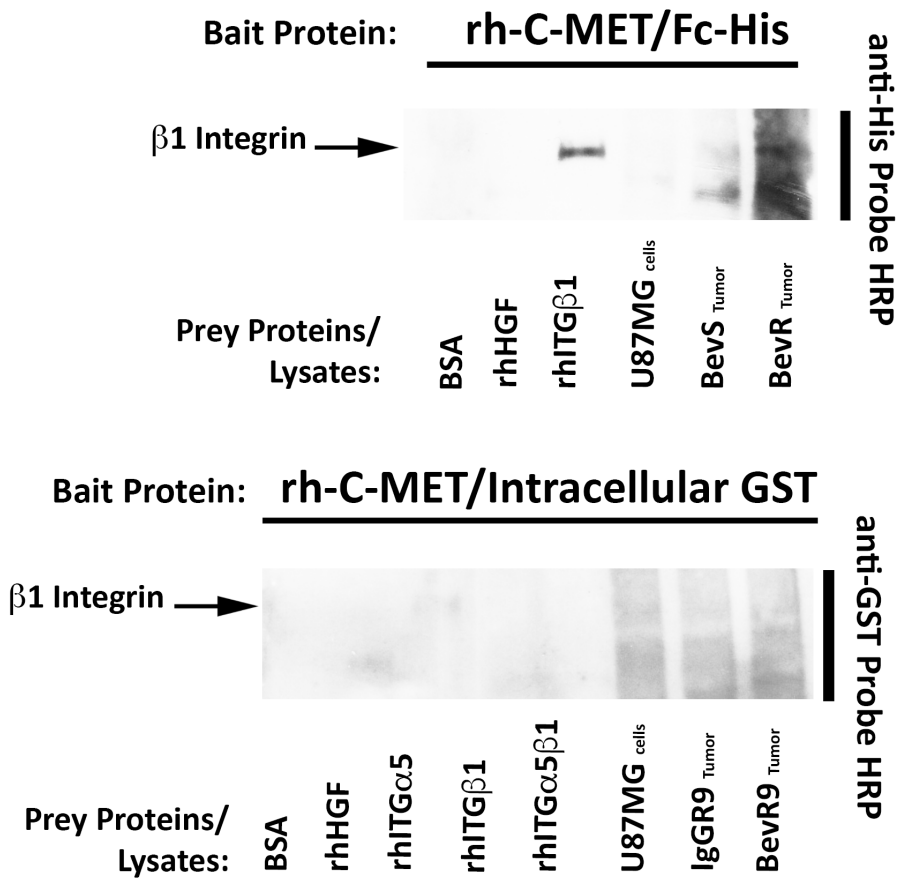

Fig. S24. Expanded far western blot of xenografts reveals more robust β1 to bind the extracellular, not the intracellular, c-Met domain in U87-Bev^R, not U87-Bev^S, xenografts. Related to **Fig. 5*B***. Expansion of far western blot from **Fig. 5*B*** showing that lysates from U87-Bev^R tumors bound exracellular, not intracellular, c-Met better than lysates from U87-Bev^S tumors or U87 parental GBM cells, likely indicating greater availability of β1 integrin in the U87-Bev^R lysates.

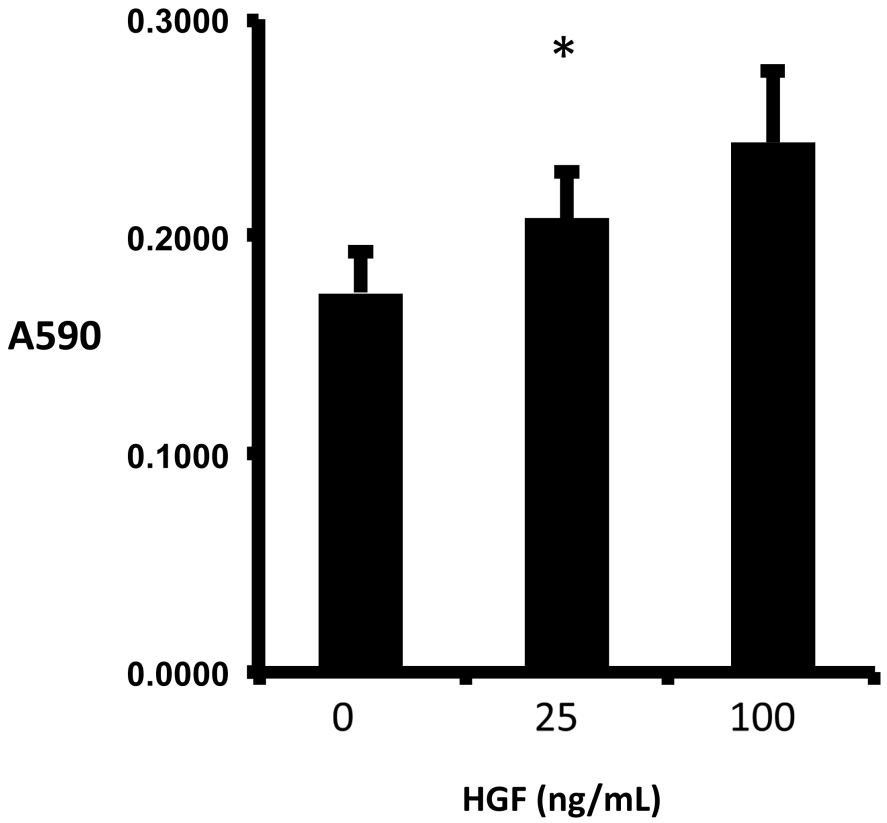

Fig. S25. Impact of HGF on adhesion of U87 cells to fibronectin. Related to **Fig. 5**. U87 cells exhibited increased adhesion to fibronectin in response to increasing HGF (P=0.02). * P<0.05; ** P<0.01 *** P<0.001.

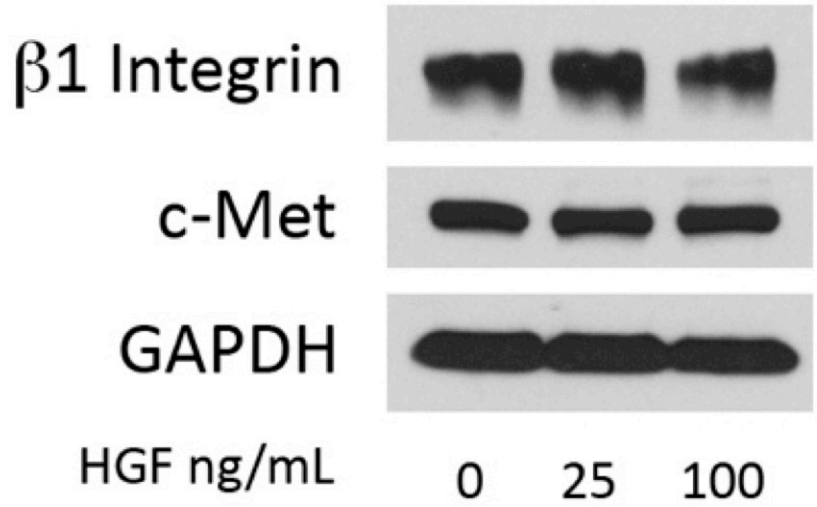

Fig. S26. HGF does not alter β1 integrin expression. Related to **Figs. 5*D* and S25**. Western blot from U87 cells exposed to the same concentrations of HGF for the same durations as in **Fig. S25** revealed no changes in β1 integrin expression, suggesting that the increased adhesion seen by western blot in **Fig. 5*D*** and by adhesion assay in **Fig. S25** reflected altered β1 integrin activation rather than expression.

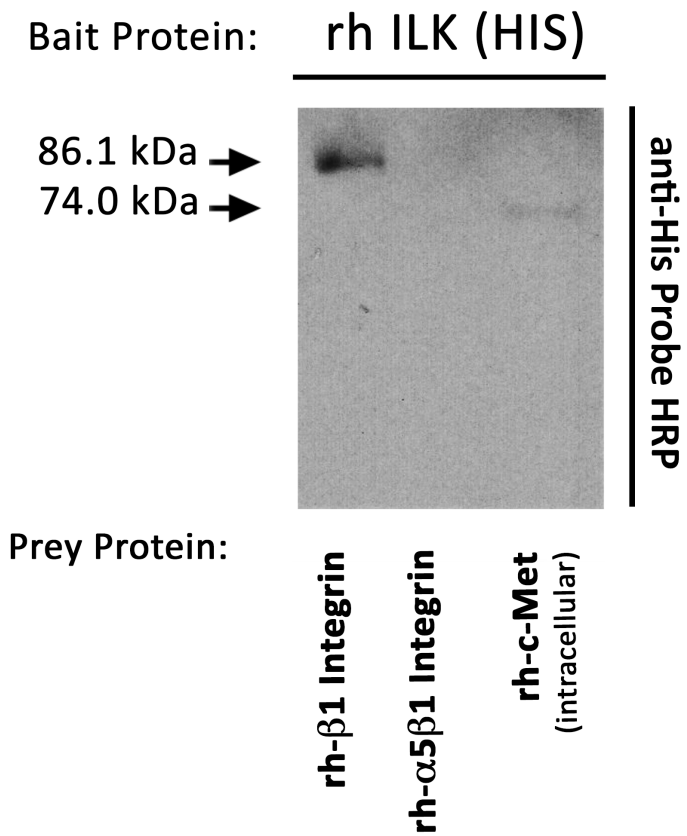

Fig. S27. ILK binds c-Met. Related to **Fig. 5**. Far western blot to assess whether ILK binds c-Met. His-tagged recombinant human ILK was bait with β1 integrin, α5β1 integrin, or c-Met as prey.

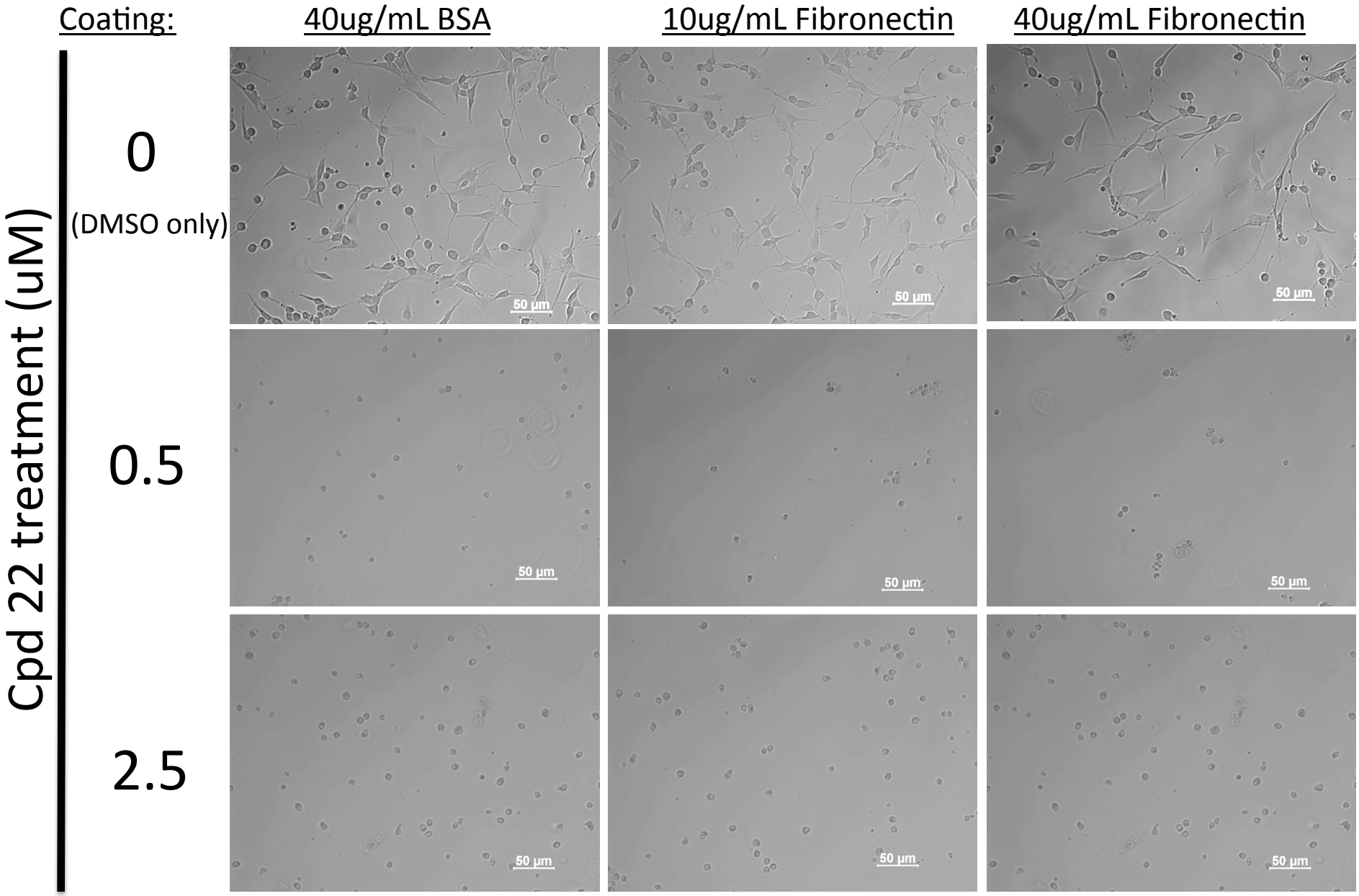

Fig. S28. Impact of ILK inhibitor on tumor cell morphology and adhesion. Related to **Fig. 5*G***. ILK inhibitor Cpd 22, which is shown in **Fig. 5*H*** to prevent fibronectin-induced c-Met phosphorylation, changed morphology of U87 cells to more circular and reduced adhesion to fibronectin. 20x magnification; scale bars 50 μm.

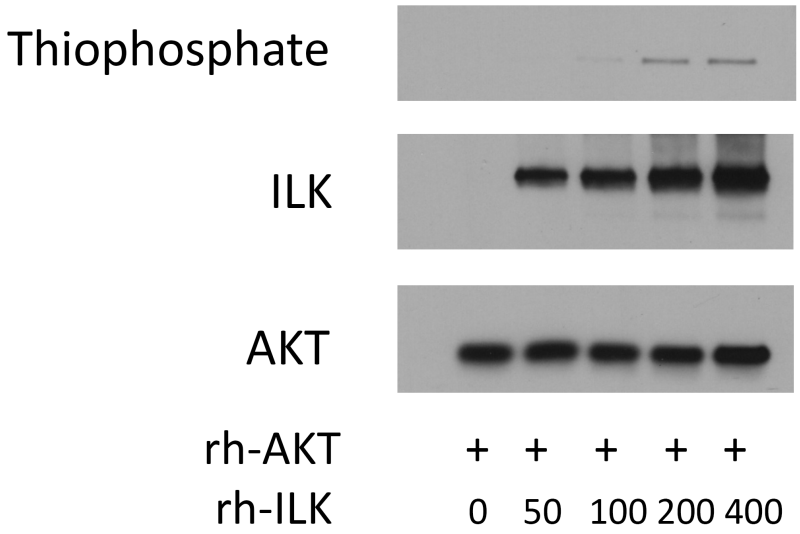

Fig. S29. ILK phosphorylates AKT. Related to **Fig. 5**. Recombinant ILK was incubated with recombinant kinase-null human AKT (ng of protein shown below each lane) and ATPγS. Thiophosphate western blotting revealed concentration-dependent increases in AKT phosphorylation.

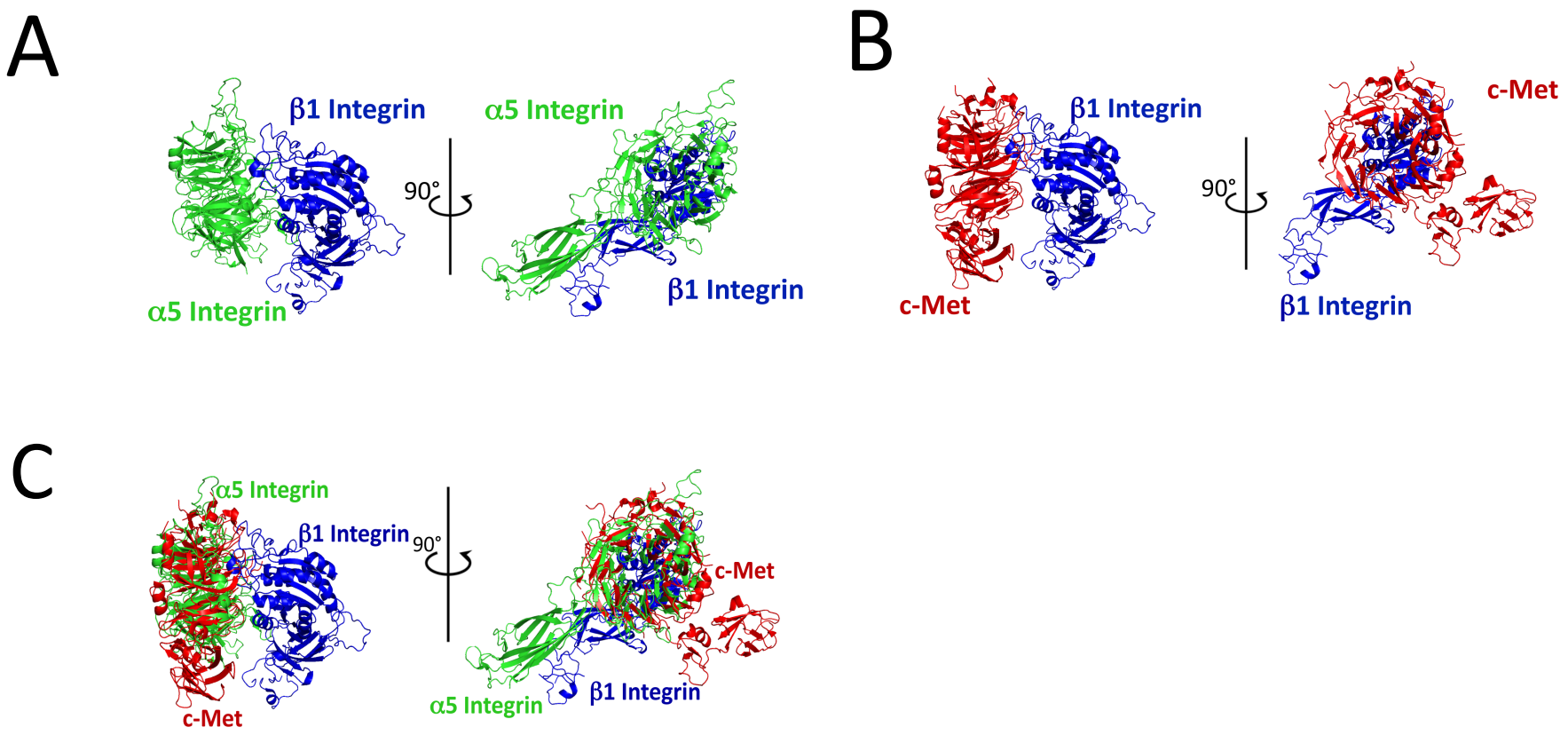

Fig. S30. Structural modeling of α5/β1 and c-Met/β1 integrin complex. Related to **Fig. 6**. PyMOL crystal structure software analysis defined (**A**) the structure of the heterodimer formed by α5 integrin (green) and β1 integrin (blue); (***B***) the structure of the c-Met/β1 complex; and (**C**) the likelihood that c-Met (red) displaces α5 (green) from its β1 (blue) binding site due to similar c-Met and α5 propeller regions.

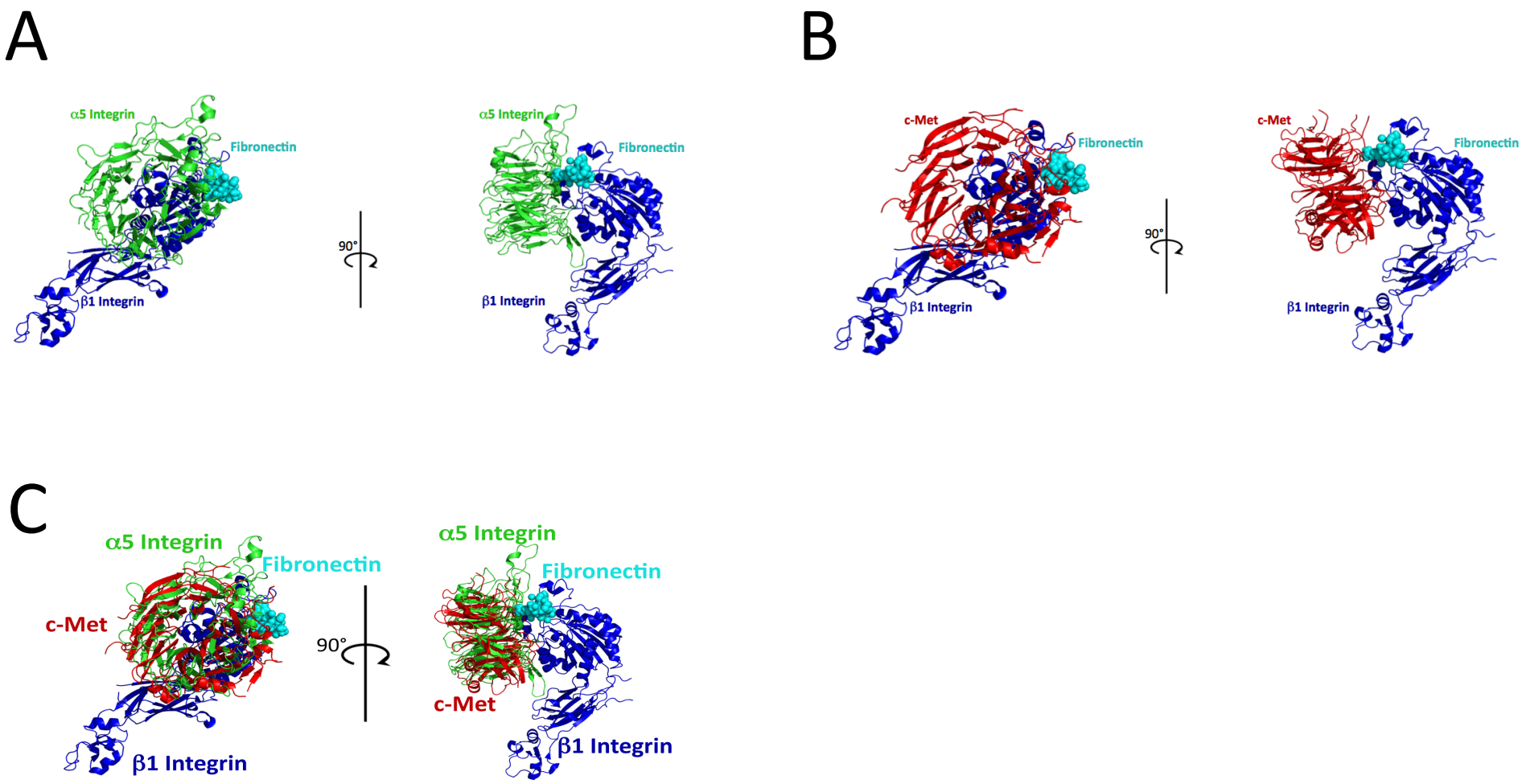

Fig. S31. Structural modeling of α5/β1 and c-Met/β1 integrin complex as they bind to fibronectin. Related to **Fig. 6**. PyMOL crystal structure software analysis defined (**A**) the structure of the heterodimer formed by α5 integrin (green) and β1 integrin (blue) as it binds to fibronectin (cyan); (**B**) the structure of the c-Met (red) and β1 complex, which creates a similar pocket allowing for fibronectin (cyan) to bind; and (**C**) the finding that c-Met, after replacing α5, binds fibronectin (cyan) through the same Arg-Gly-Asp motif as α5.

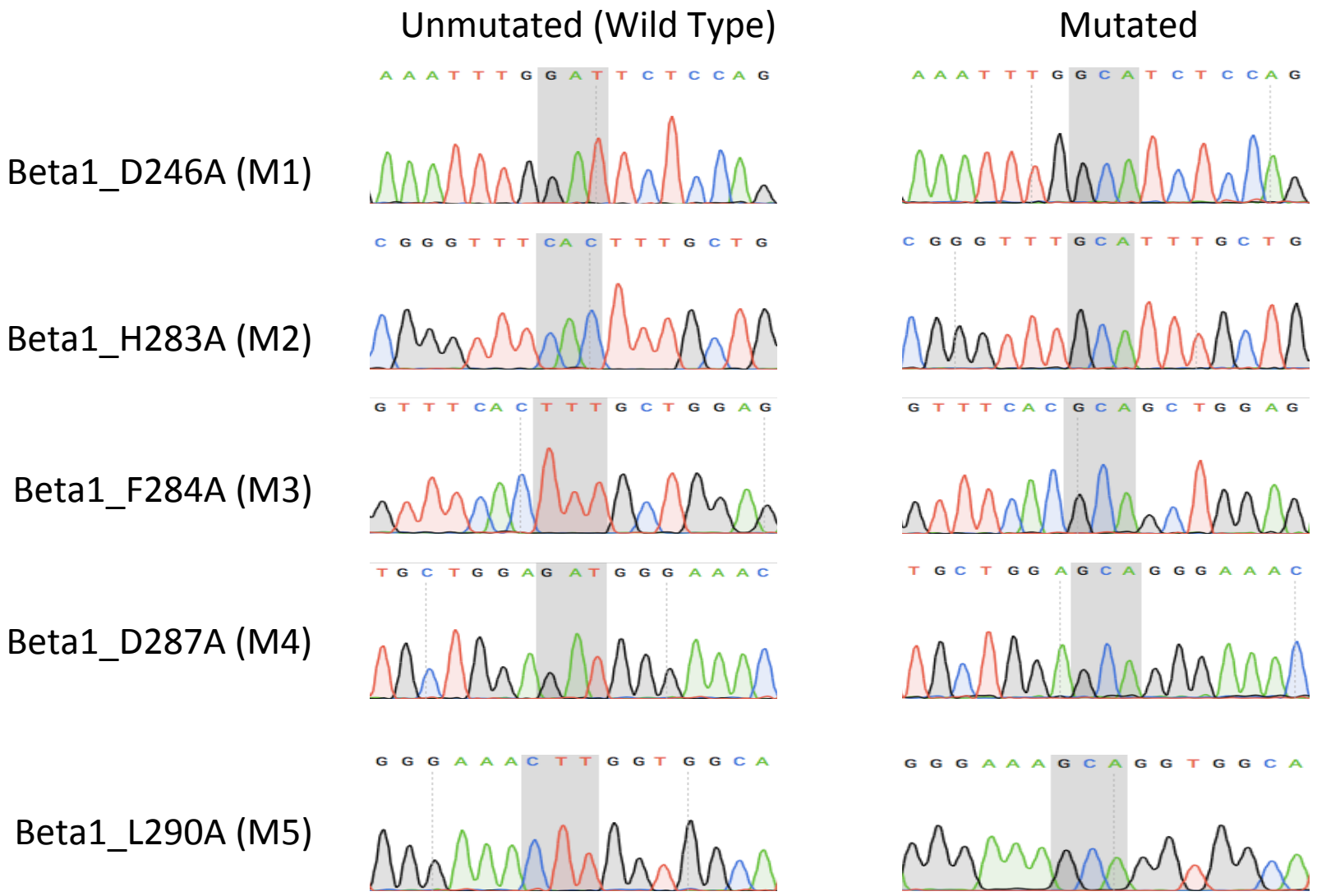

Fig. S32. Sequencing results from engineered mutations in β1 integrin created to disrupt c-Met/β1 integrin binding based on results of PyMOL modeling. Related to **Fig. 6*F***. Based on PyMOL crystal structure software analysis, the Rosetta ALA scanning method was used to determine predicted changes in delta-delta-G that would arise by disrupting specific amino acids in β1 integrin, with higher scores associated with more loss of c-Met/β1 integrin binding. The 3 nucleotides coding for the amino acids with the five highest scores were converted from their original sequence to 'GCA' in order to obtain alanine residues, with the resulting sequence changes shown here.

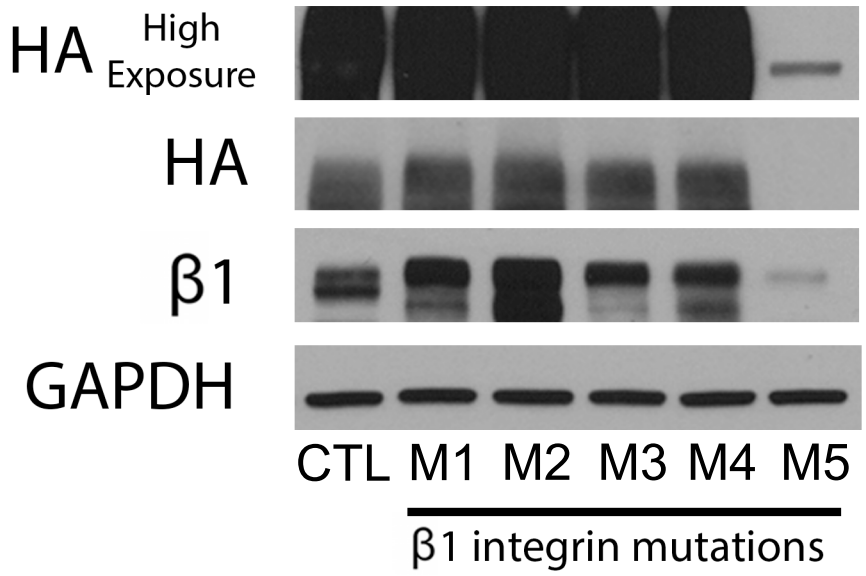

Fig. S33. Whole cell lysates from HEK cells expressing wild type β1 integrin-HA fusion protein and five mutant β1 integrin-HA fusion proteins. Related to **Fig. 6*F***. The five β1 integrin mutations suggested by PyMOL crystal structure software and the Roseta ALA method were created in a β1 integrin-HA fusion protein with the resulting cDNAs transfected into HEK cells. After cell selection, whole cell lysates underwent western blotting for the proteins shown above. The presence of the HA tag was confirmed in HEK cells expressing wild type β1 integrin-HA fusion protein and the five mutations, with the M5 mutation-HA fusion protein less robustly expressed than wild type protein or mutations M1-M4, such that a higher exposure was required to visualize HA in HEK cells expressing the M5-HA fusion protein.

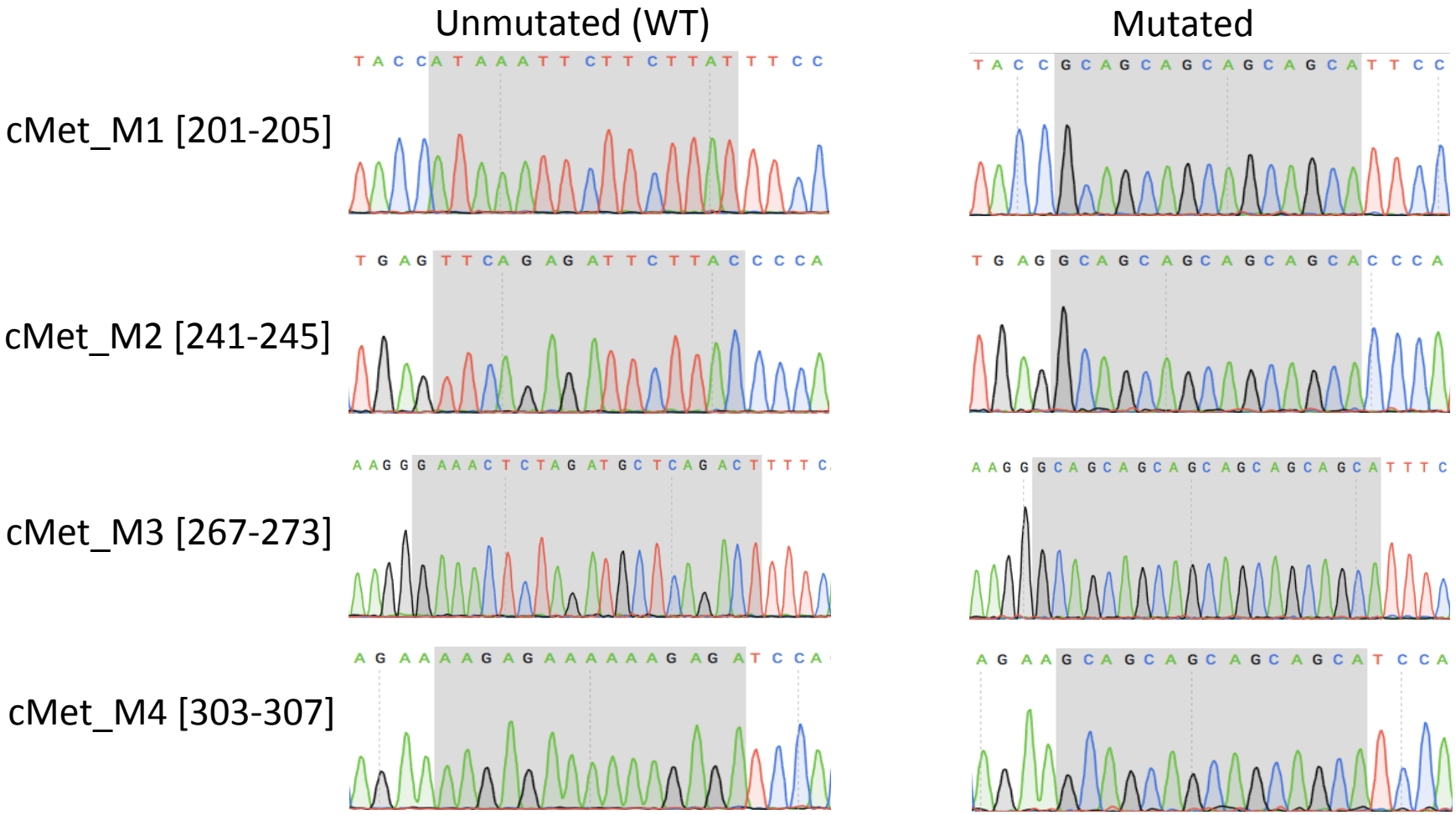

Fig. S34. Sequencing results from engineered mutations in c-Met created to disrupt c-Met/β1 integrin binding based on PyMOL modeling. Related to **Fig. 6**. Because the Rosetta ALA scanning method could not be used to predict changes in delta-delta-G that would arise by disrupting specific amino acids in c-Met due to the model interface not being sufficiently accurate, based on PyMOL analysis predicting that the loops on the top of the 7-bladed β-propeller domain of c-Met would contact β1 integrin, we investigated whether disrupting these loops atop the β-propeller domain of c-Met would affect c-Met/β1 integrin binding. The nucleotides coding for the amino acids in four of these five loops were converted from their original sequences to a series of 'GCA's in order to obtain alanine residues, with the resulting sequence changes shown here. The genetic change required to alter the fifth loop in amino acids 348-359 failed to be established correctly after multiple attempts at mutagenesis and sequencing and was thus not used.

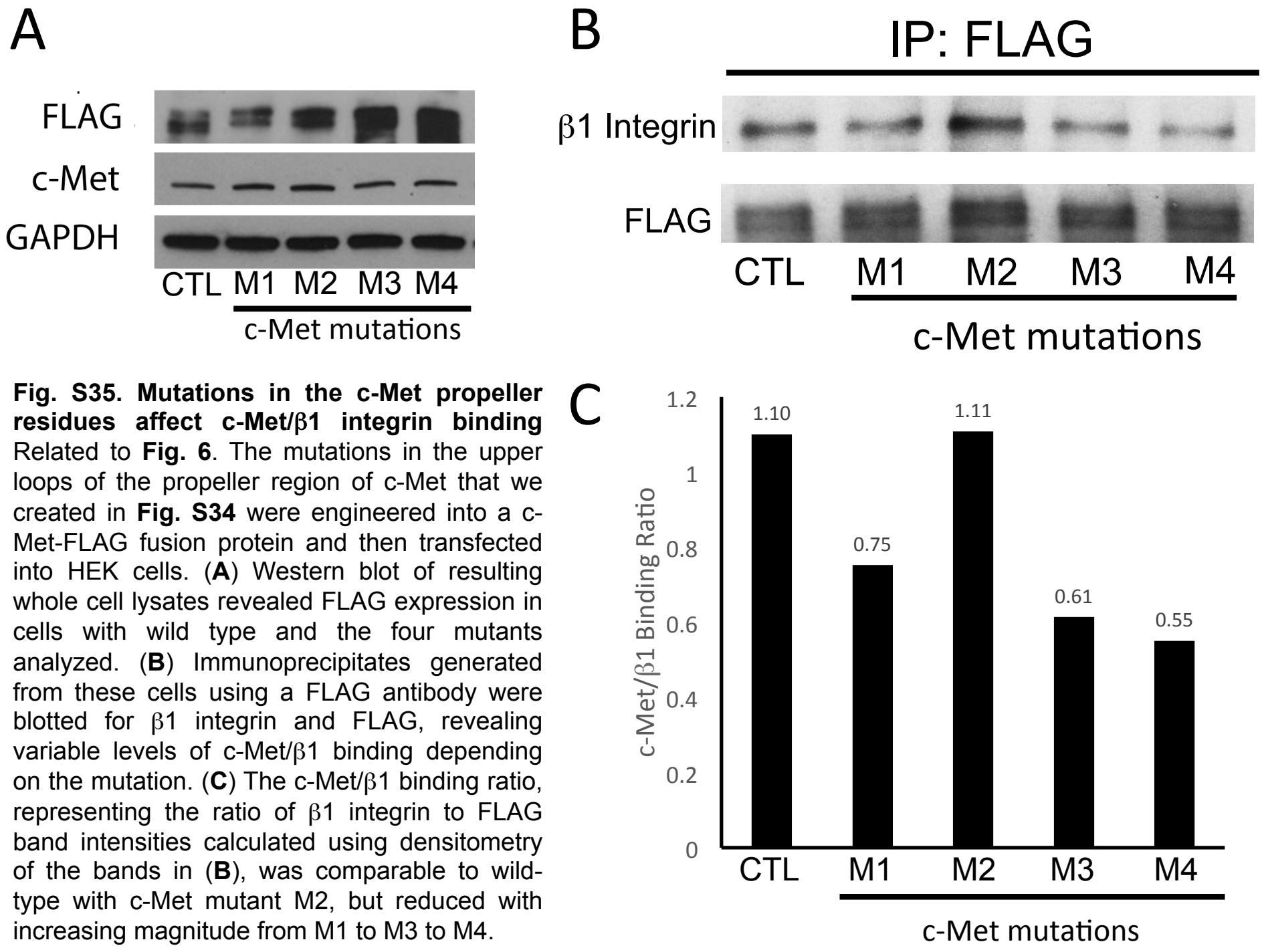

Fig. S35. Mutations in the c-Met propeller residues affect c-Met/β1 integrin binding Related to **Fig. 6**. The mutations in the upper loops of the propeller region of c-Met that we created in **Fig. S34** were engineered into a c-Met-FLAG fusion protein and then transfected into HEK cells. (**A**) Western blot of resulting whole cell lysates revealed FLAG expression in cells with wild type and the four mutants analyzed. (**B**) Immunoprecipitates generated from these cells using a FLAG antibody were blotted for β1 integrin and FLAG, revealing variable levels of c-Met/β1 binding depending on the mutation. (**C**) The c-Met/β1 binding ratio, representing the ratio of β1 integrin to FLAG band intensities calculated using densitometry of the bands in (**B**), was comparable to wild-type with c-Met mutant M2, but reduced with increasing magnitude from M1 to M3 to M4.

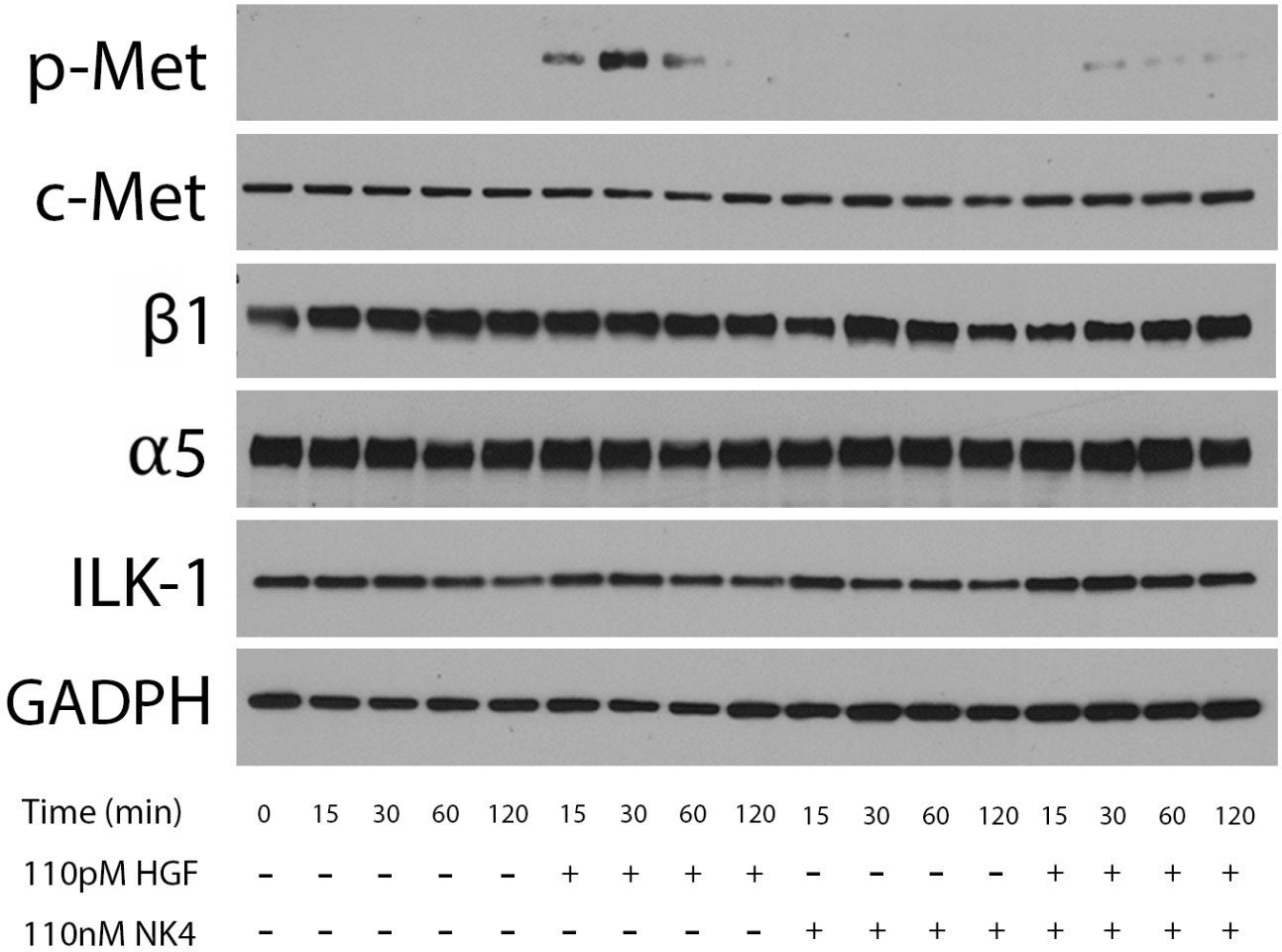

Fig. S36. Effect of c-Met/HGF therapeutic antagonist NK4 on c-Met phosphorylation. Related to **Fig. 6**. Cultured U87 cells were treated with 110 pM HGF and/or 110 nM of c-Met/HGF therapeutic antagonist NK4 for varying times. Western blots of whole cell lysates revealed that HGF led to c-Met phosphorylation peaking at 30 minutes, while NK4 did not affect c-Met phosphorylation and adding NK4 to HGF led to a diminished level of c-Met phosphorylation compared to HGF alone.

A

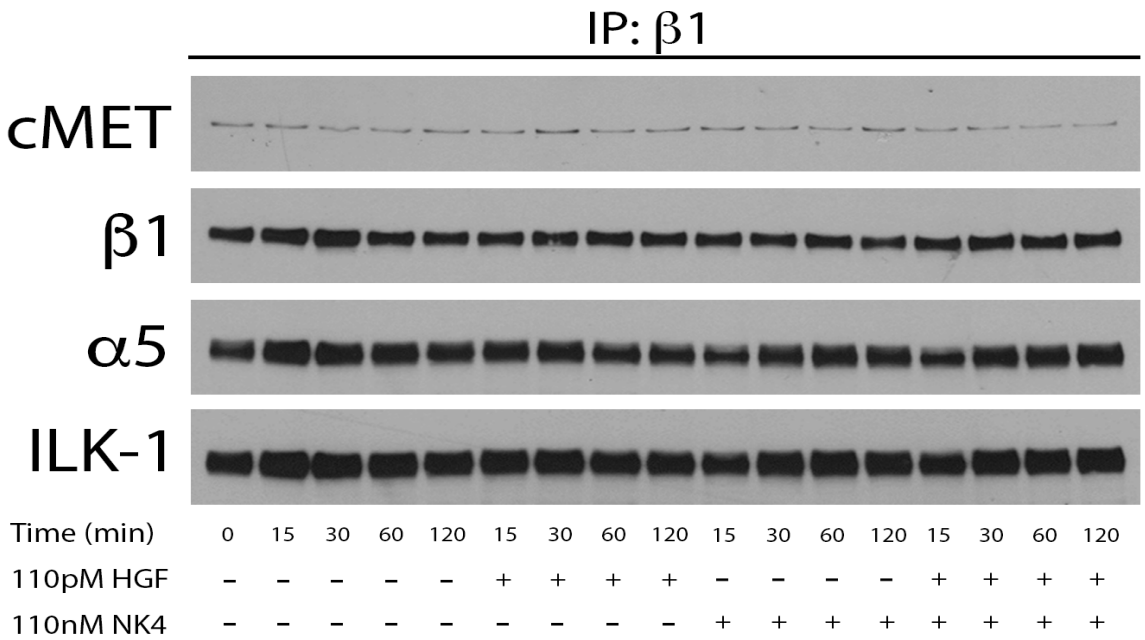

B

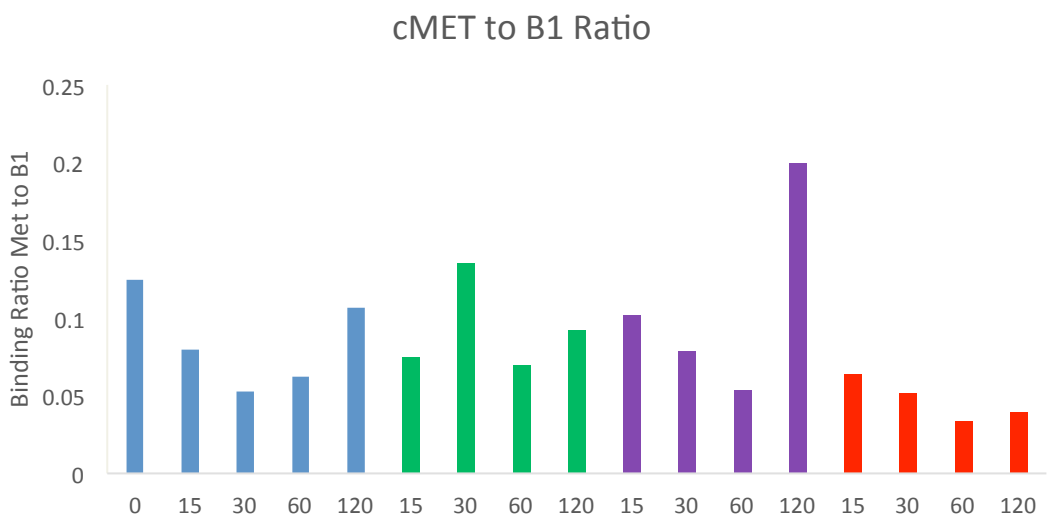

Fig. S37. Effect of c-Met/HGF therapeutic antagonist NK4 on c-Met/β1 complex formation. Related to **Fig. 6**. Cultured U87 cells were treated with 110 pM HGF and/or 110 nM of c-Met/HGF therapeutic antagonist NK4 for varying times. Immunoprecipitation for β1 integrin followed by blotting of the precipitates revealed that HGF increased c-Met/β1 integrin complex formation at 30 minutes, corresponding to the time at which HGF induced c-Met phosphorylation. NK4 alone was associated with a delayed 120 minute spike in c-Met/β1 integrin complex formation, but adding NK4 to HGF suppressed HGF-induced complex formation.

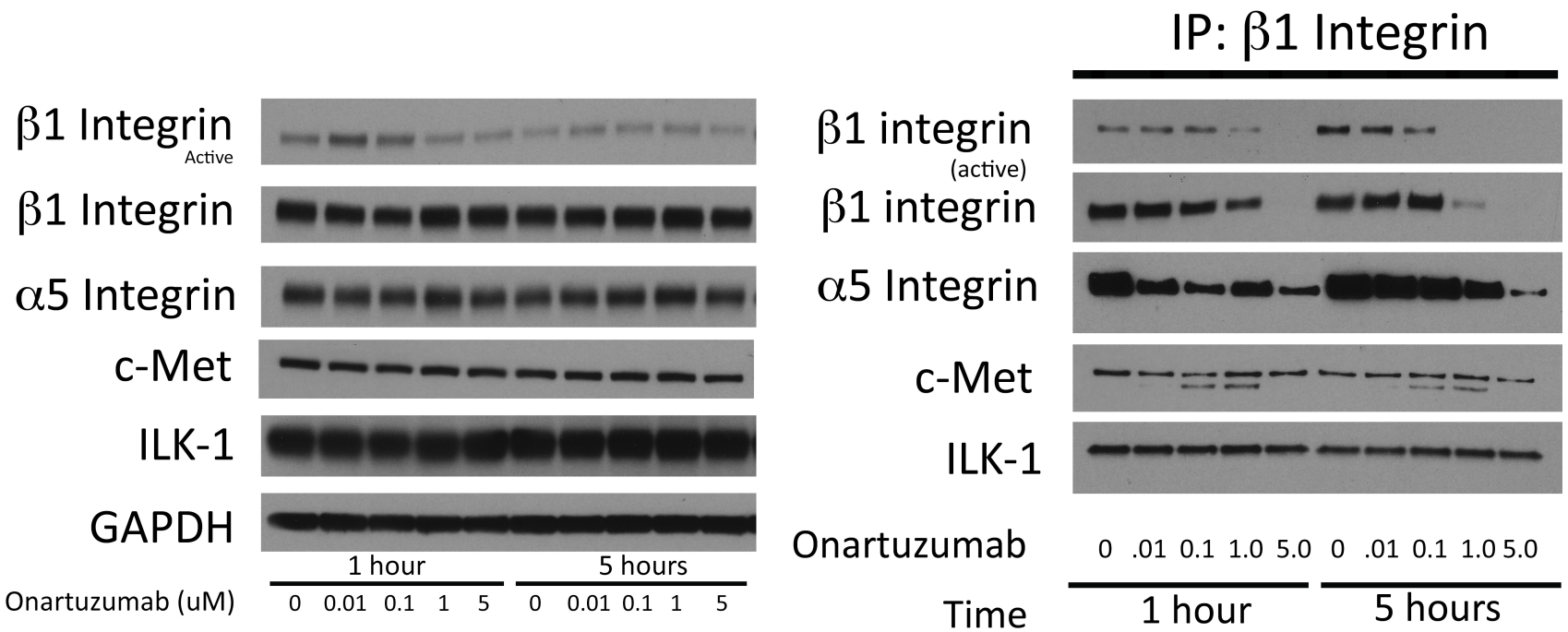

Fig. S38. Effect of c-Met neutralizing antibody onartuzamab on c-Met/β1 complex formation. Related to **Fig. 6**. Cultured U87 cells were treated with varying concentrations of c-Met neutralizing antibody onartuzamab for 1 and 5 hours. (A) Western blots of whole cell lysates from these cells revealed that onartuzamab reduced levels of activated β1 without affecting levels of β1 integrin detected with antibody ab52971 which reacts to an epitope spanning β1 amino acids 650-750, outside of the predicted area in β1 integrin that interacts with c-Met. (B) immunoprecipitation of these lysates with b1 integrin antibody ab7168 which binds extracellular b1 at an unknown epitope) revealed decreased binding of ab52971 to β1 integrin in the precipitates. This finding together with the whole cell lysate western blot result suggests that onartuzamab blocked the ability of ab7168 to detect its β1 integrin epitope, suggesting that ab7168's epitope falls in the β1 amino acids predicted to bind c-Met (amino acids 246-290). Unfortunately, because ab52971 was the only antibody which produced a clean blot on the precipitates, an IP revealing the unchanged β1 integrin levels seen in the whole cell lysates could not be rendered, making it difficult to discern the impact of onartuzamab on c-Met/β1 binding. But the effect of onartuzamab on the ability of ab7168 and ab24693 to bind their β1 epitopes offered insight into c-Met/β1 binding domains.

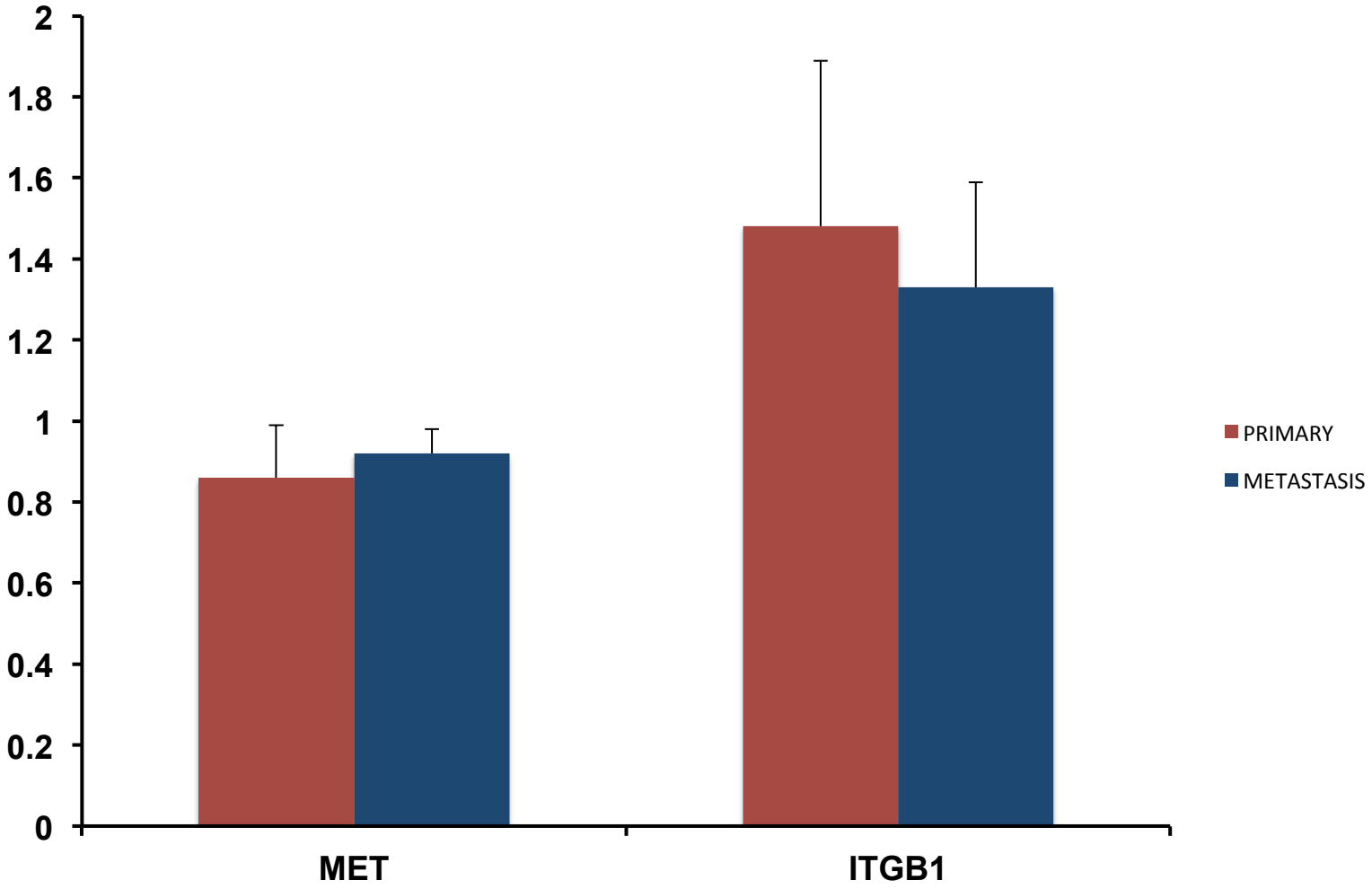

Fig. S39. Microarray analysis of c-Met and β1 integrin expression in paired primary and metastatic breast cancer. Related to **Fig. 7**. Analysis of publically deposited microarray data revealed no change in c-Met (P=0.3) or β1 integrin (P=0.4) expression in paired metastases and primary breast tumors (n=8 pairs).

SF9416 whole lysate westerns

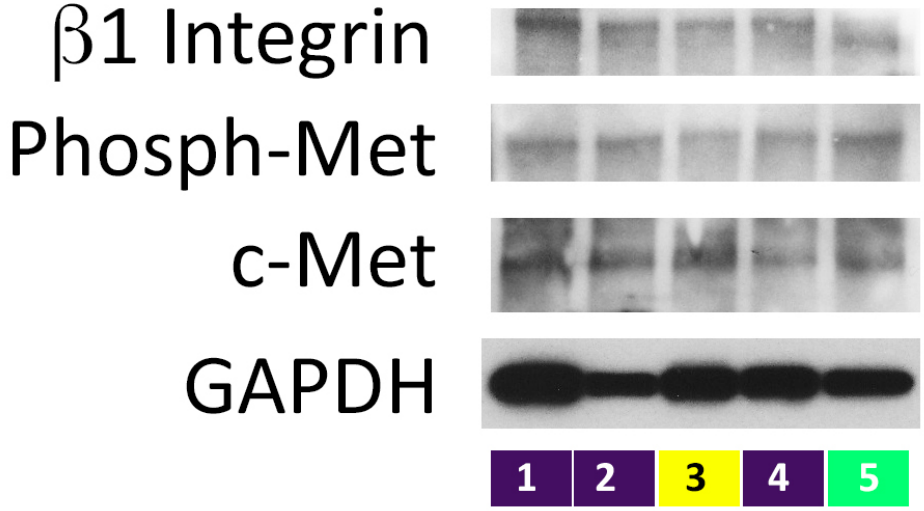

order of western based on real nomenclature from O.R.
2_4_1_5_3

Fig. S40. Western blots of lysates from site-directed biopsies of bevacizumab-resistant GBM. Related to **Fig. 8*A***. Protein lysates from each location in **Fig. 8*A*** were immunoblotted for the antigens shown here.

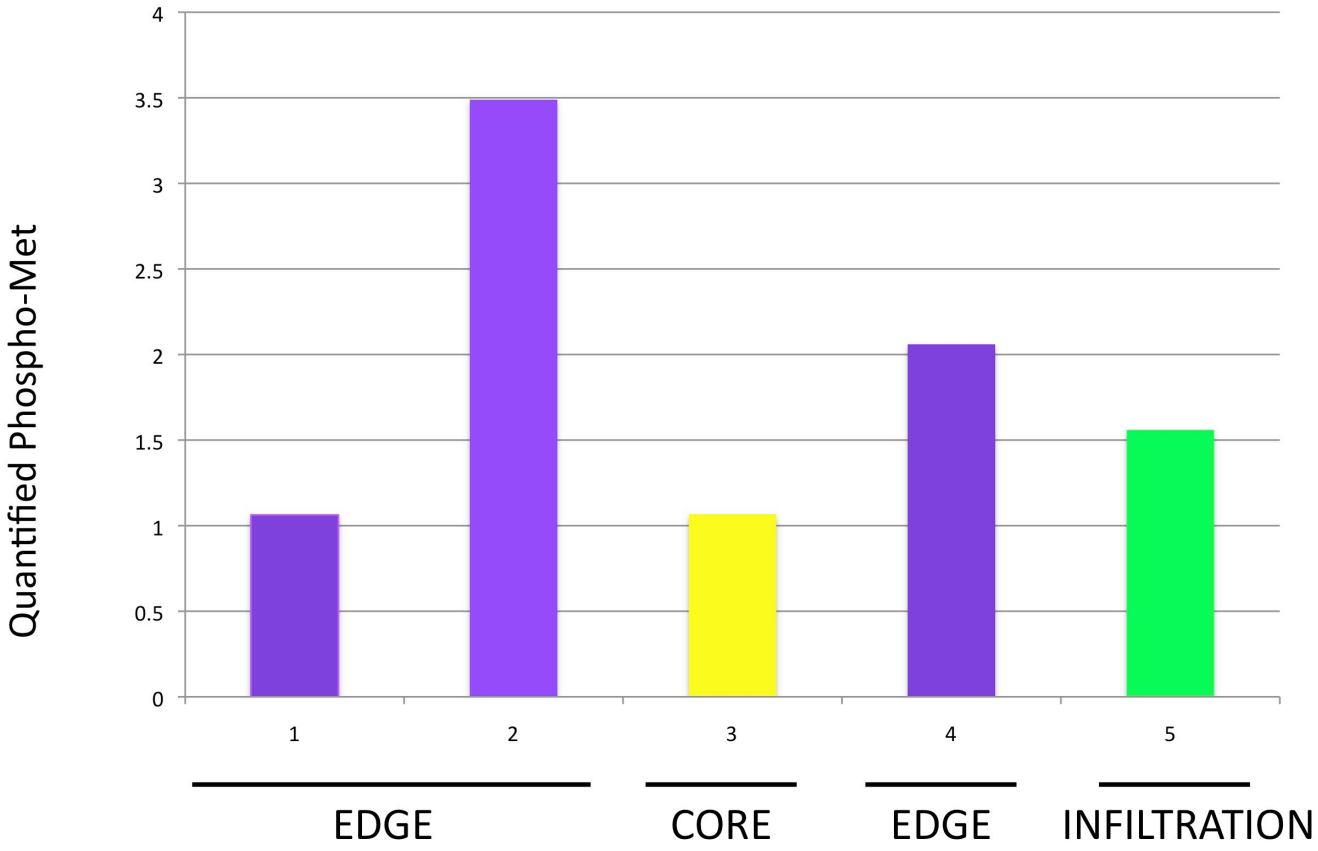

Fig. S41. Quantified levels of phosphorylated c-Met bound to β1 integrin. Related to **Fig. 8*A***. Protein lysates from each location in **Fig. 8*A*** were used for immunoprecipitation with β1 integrin and immunoblotted for phosphorylated c-Met, quantified, and its levels shown.

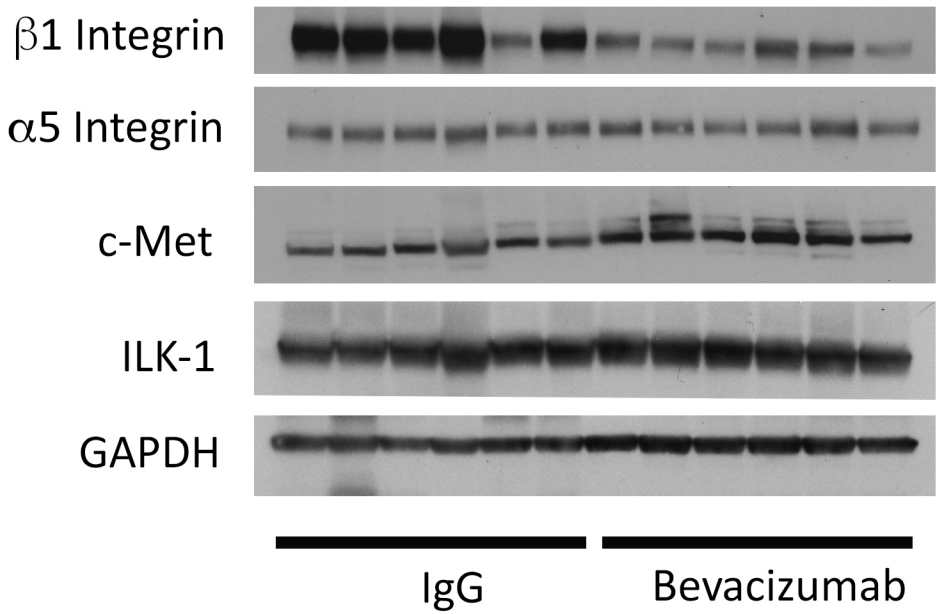

Fig. S42. Western blots of lysates from patient-derived xenografts derived from bevacizumab-resistant GBM. Related to **Fig. 8*C***. Protein lysates from each xenograft in **Fig. 8*C*** were immunoblotted for each of the antigens shown here. Note that bevacizumab reduced the ability of rabbit ab52971 to recognize β1 integrin in the whole cell lysates as occurred in **Fig. S13** but no such issues occurred with the combination of antibodies used in the IP in **Fig. 8*C***.

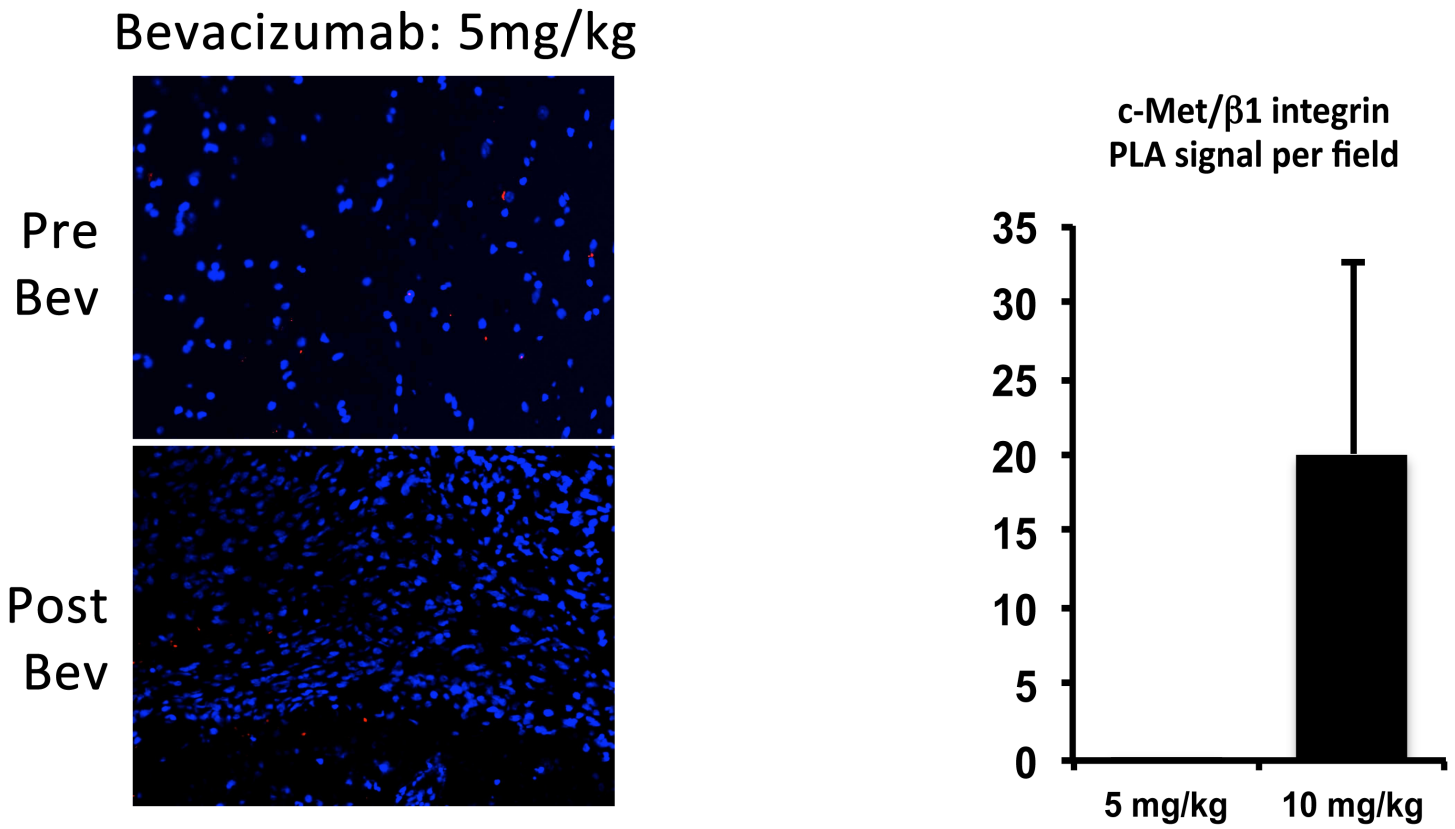

Fig. S43. Complex formation occurs in a dose-dependent manner in bevacizumab-resistant patient GBM specimens. Related to **Fig. 7**. PLA from a patient treated with 5 mg/kg bevacziumab twice weekly revealed decreased c-Met/β1 integrin complex relative to pre-treatment, unlike the increase seen at 10 mg/kg (same cases analyzed in **Fig. 7*B***).

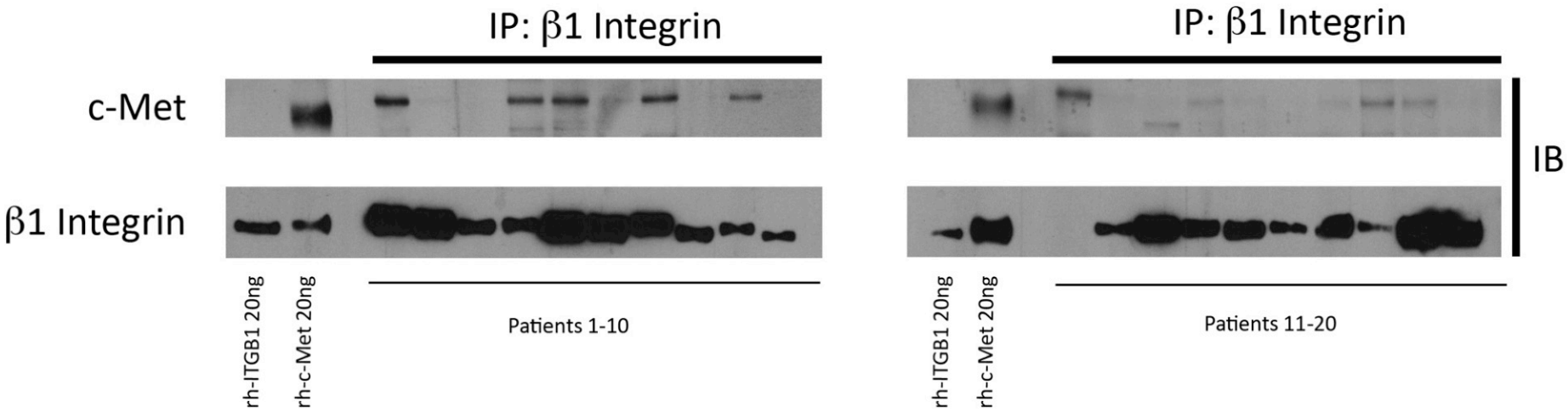

Fig. S44. Immunoprecipitation to quantify c-Met/β1 integrin complex in protein lysates from newly diagnosed glioblastomas. Related to **Fig. S45**. Band densitometries of c-Met pulled down in a β1 IP were normalized relative to the intensity of 20 ng of purified c-Met and then divided by the band intensity of β1 integrin in the IP normalized to the intensity of 20 ng of purified β1 integrin. The result, reflecting percentage of β1 integrin bound to c-Met, correlated inversely with survival as illustrated in **Fig. S45**.

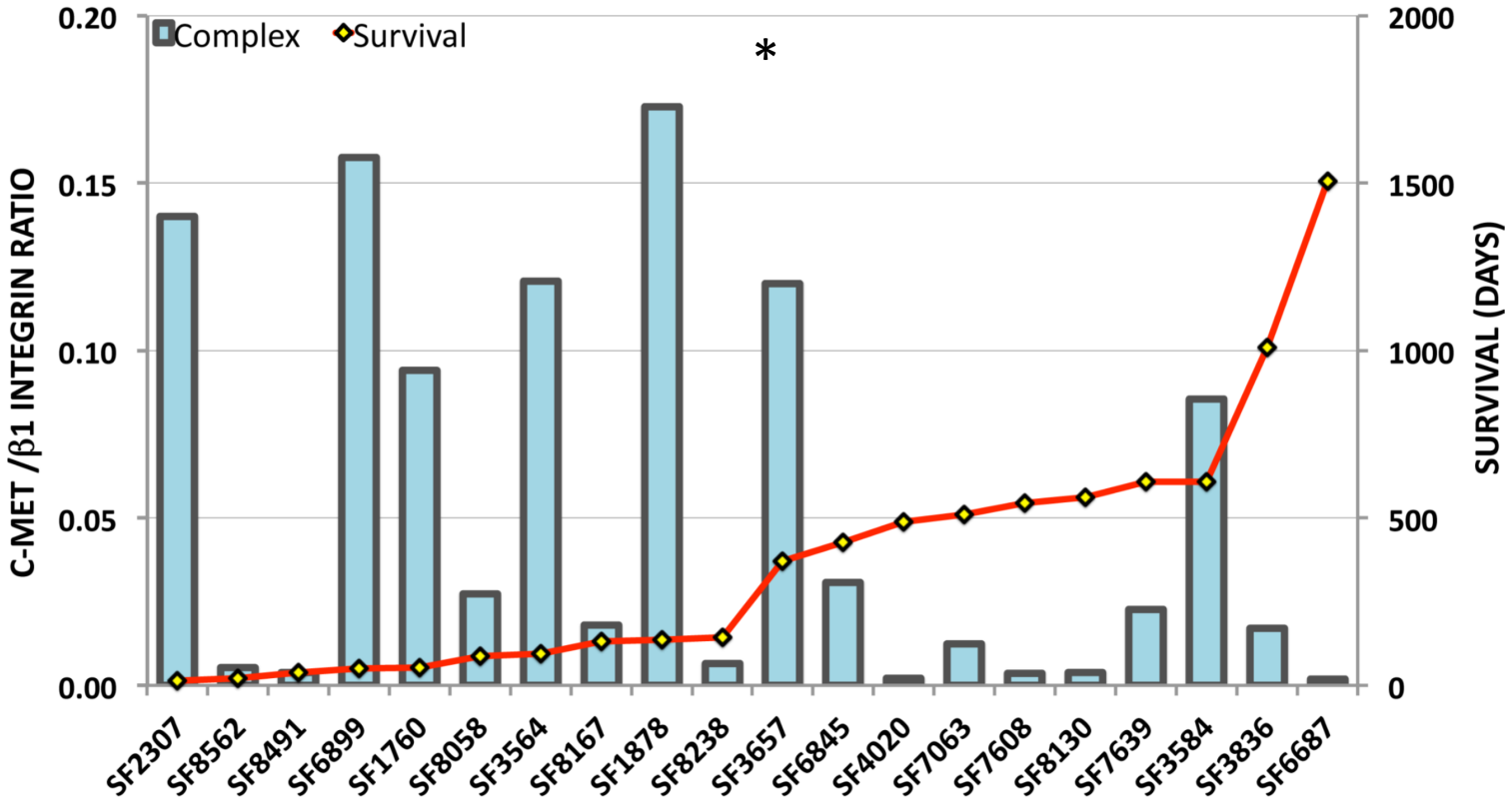

Fig. S45. Immunoprecipitation to quantify c-Met/β1 integrin complex in protein lysates from newly diagnosed glioblastomas. Related to **Fig. S44**. 20 GBM patients presented in order of increasing survival (right-hand vertical axis, red line graph) after diagnosis. Levels of c-Met/β1 integrin protein complex from lysates of tumors resected at diagnosis, normalized to recombinant levels (IP results shown in **Fig. S44**), are presented in blue bar graphs with complex levels noted on the left y-axis (P<0.05). * P<0.05; ** P<0.01 *** P<0.001.

Supplemental Table S1. Amino acids targeted by antibodies and engineered mutations used in this study.

Antibody (purpose)	**Human Antigen**	**Amino acids targeted**	**Technical issues arising with results**
Onartuzamab (therapeutic)	c-Met	328, 331, 337, 338 (Sema domain)	None
OS2966 (therapeutic)	β1 integrin	211 (β1 βI domain)	None
ab52971 (research)	β1 integrin	650-750	Bevacizumab, but not onartuzamab, affected ability of ab52971 to detect β1 integrin in cultured U87 cells.
ab7168 (research)	β1 integrin	Extracellular domain (exact amino acids unknown)	Onartuzamab, but not bevacizumab, affected ability of ab7168 to detect β1 integrin in cultured U87 cells
ab24693	β1 integrin	Exact amino acids unknown	Onartuzamab, but not bevacizumab, affected ability of ab24693 to detect β1 integrin in cultured U87 cells
Engineered Mutation	**cDNA**	**Amino acids targeted**	**Notes from results**
c-Met mutation #1	c-Met-FLAG	201-205	None
c-Met mutation #2	c-Met-FLAG	241-245	None
c-Met mutation #3	c-Met-FLAG	267-273	None
c-Met mutation #4	c-Met-FLAG	303-307	None
Proposed c-Met #5	c-Met-FLAG	348-359	Could not successfully alter this part of the sequence
β1 mutation #1	β1 integrin-HA	246	None
β1 mutation #2	β1 integrin-HA	283	None
β1 mutation #3	β1 integrin-HA	284	None
β1 mutation #4	β1 integrin-HA	287	None
β1 mutation #5	β1 integrin-HA	290	None

Supplemental Table S2. Antibodies used in these studies. Shown are antibodies used in their studies, their specific usage, species of origin, dilution used, and vendor/catalog number.

Antigen	Usage	Species	Dilution	Provider	Catalog #
β_1 Integrin (human)	Immunoprecipitation	Rabbit-Monoclonal	1:20	Abcam	ab52971
β_1 Integrin (human)	Immunoblotting	Rabbit-Monoclonal	1:1000	Abcam	ab51729
β_1 Integrin (human)	Immunoblotting	Mouse-Monoclonal	1:1000	Abcam	ab24693
β_1 Integrin (human)	Immunoblotting	Rabbit-Polyclonal	1:1000	Cell Signaling	4706
β_1 Integrin (human)	Immunohistochemistry (PLA)	Mouse-Monoclonal	1:100	Abcam	ab30394
c-Met (Human)	Immunoblotting	Rabbit-Monoclonal	1:1000	Abcam	ab51067
c-Met (Human)	Immunoblotting	Mouse Monoclonal	1:1000	Cell Signaling	3148
c-Met (Human)	Immunohistochemistry (PLA)	Rabbit-Monoclonal	1:250	Abcam	ab51067
p-MET (Tyr1234/ 1235; Human)	Immunoblotting	Rabbit-Monoclonal	1:1000	Cell Signaling	3126
ILK (human)	Immunoblotting	Rabbit-Monoclonal	1:1000	Cell Signaling	3856
α_5 Integrin (human)	Immunoblotting	Rabbit-Monoclonal	1:1000	Cell Signaling	54705
Thio-phosphate	Immunoblotting	Rabbit-Monoclonal	1:2000	Abcam	ab92570
AKT1 (human)	Immunoblotting	Rabbit-Monoclonal	1:1000	Cell Signaling	2138
Vimentin (human)	Immunohistochemistry	Rabbit-Monoclonal	1:250	Abcam	ab16700
Activated β1 integrin (human)	Immunoblotting	Mouse-Monoclonal	1:1000	Millipore	MAB20792
GAPDH	Immunoblotting	Mouse-Monoclonal	1:50,000	Millipore	MAB374
α1 integrin (human)	Immunoblotting	Mouse-Monoclonal	1:1000	Millipore	MAB1973
α2 integrin (human)	Immunoblotting	Rabbit Monoclonal	1:1000	Cell Signaling	13807
α3 integrin (human)	Immunoblotting	Rabbit	1:1000	Millipore	MAB1920

α4 integrin (human)	Immunoblotting	Rabbitt	1:1000	Cell Signaling	4600
α5 integrin (human)	Immunoblotting	Rabbitt	1:1000	Cell Signaling	4705
α6 integrin (human)	Immunoblotting	Rabbitt	1:1000	Cell Signaling	#3750
αV integrin (human)	Immunoblotting	Rabbitt	1:1000	Cell Signaling	4711
β3 integrin (human)	Immunoblotting	Rabbitt	1:1000	Cell Signaling	4702
β4 integrin (human)	Immunoblotting	Rabbitt	1:1000	Cell Signaling	4707
β5 integrin (human)	Immunoblotting	Rabbitt	1:1000	Cell Signaling	4708
Human VCAM	Immunoblotting	Rabbitt	1:1000	Cell Signaling	13662
Human Osteo-pontin	Immunoblotting	Rabbitt	1:1000	Abcam	ab8448
Human phosphorylated VEGFR2 (Tyr1175)	Immunoblotting	Rabbitt	1:1000	Cell Signaling	2478

Supplemental Table S3. Plasmids and constructs used in these studies. Shown are plasmids, their usage, and the source from which they were obtained.

Plasmid Name	Usage	Source
pRK5-ITGB1	Used as source cDNA to create integrin β_1 PCR fragments for cloning	Addgene®
pENTR-D-TOPO-cMET	Used as source cDNA to amplify *MET* PCR fragments	Addgene®
pLVX-Het1-DmrC	Part of Clontech Lenti-X iDimerize™ plasmid kit	Clontech®
pLVX-Het2-DmrA	Part of Clontech Lenti-X iDimerize™ plasmid kit	Clontech®
pCR4-Blunt-TOPO	Topoisomerase cloning of blunt PCR products	Invitrogen®
pCR4- β_1-HA	HA-tagged integrin β_1 cDNA	Author Generated
pCR4-cMET-His	6xHis-tagged *MET* cDNA	Author Generated
pLVX-Het1-β_1-HA	HA-tagged integrin β_1 lentiviral construct for constitutive expression	Author Generated
pLVX-Het1-β_1	Integrin β_1 lentiviral construct for constitutive expression	Author Generated
pLVX-Het2-cMET	Lentiviral construct for stable expression of DmrA-fused *MET*	Author Generated
pLVX-Het2-cMET-His	Lentiviral construct for stable expression of DmrA-fused *MET* with 6xHis tag	Author Generated
pLVX-Het2-cMET-FLAG	Lentiviral construct for stable expression of DmrA-fused *MET-FLAG*	Author Generated

Supplemental Table S4. Primers used in the studies. Shown are forward and reverse primers, their usage, and their sequences.

Primer Name	Use	Sequence 5' to 3'
B1(NotI)Fw	Amplification of ITGB1 cDNA from pRK5-Beta1 conserving in-frame status with pLVX-Het1-DmrC at the 3' MCS and NotI restriction site	CTCGATTGCGGCCG CATGAATTTACAACC AATTTTCTG
B1(BamHI) RV	Amplification of ITGB1 cDNA from pRK5-Beta1 conserving in-frame status with pLVX-Het1-DmrC at the 3' MCS and BamHI restriction site	GAAATTAGGATCCTT TTCCCTCATACTTCG GAT
B1(BamHI)-HA RV	Amplification of ITGB1 cDNA from pRK5-Beta1 conserving in-frame status with pLVX-Het1-DmrC at the 3' MCS with the addition of hemagglutinin tag sequence and BamHI restriction site.	GAAATTAGGATCCAG CGTAATCTGGAACAT CGTATGGGTATTTTC CCTCATACTTCGGAT
cMET(NotI)-FW	Amplification of cMET cDNA from pENTR-cMET conserving in-frame status with pLVX-Het2-DmrA at the 3' MCS with the addition of NotI restriction site.	GCCGACGGCGGCCG CATGAAGGCCCCCG CTGTGCT
cMET(NotI)-RV		GTCATCAGCGGCCG CTTGATGTCTCCCAG AAGGAGGCT
cMET(NotI)-His RV	Amplification of cMET cDNA from pENTR-cMET conserving in-frame status with pLVX-Het2-DmrA at the 3' MCS with the addition of 6xHis amino acid sequence and NotI restriction site.	GTCATCAGCGGCCG CTGTGGTGGTGGTG GTGGTGTGATGTCTC CCAGAAGGAGGCT
cMET-pLVX2-FW	Amplification of cMET cDNA with primers containing 15bps of pLVX-Het2-DmrC arms for Gibson assembly at the 3' MCS utilizing NotI digestion.	AGCTTCTAAAACTGG AAAGCATGAAGGCC CCCGCTGTGCT
cMET-pLVX2-RV		GGCGGTCATACGTA GGATGATGTCTCCCA GAAGGAGGCT
FKBP-cMET_PCR7-FW	Amplification of fusion region between FKBP(Het2-DmrA)-cMET - forward primer in FKBP and reverse primer in cMET such that amplification only occurs in cells with the iDimerize™ system, used to quantify metastatic breast cancer cells expressing the iDimerize™ system in the lungs after tail vein injection of these cells into mice.	CCACATGCCACTCTC GTCTTC
FKBP-cMET_PCR7-RV		GTTTCCGCGGTGAA GTTGG
cMet_Mut1_FW	Mutagenesis primers designed using NEB	AGCAGCATTCCCAG ATCATCCATTG

cMet_Mut1_RV	BaseChanger software to replace specified strings of amino acids (**Supplemental Table S1**) to alanine residues in pLVX-Het-MET-FLAG.	GCTGCTGCGGTATTGCCTACAAAGAAG
cMet_Mut2_FW		AGCAGCACCCATTAAGTATGTCCATG
cMet_Mut2_RV		GCTGCTGCCTCAGGTAAAACATCAATG
cMet_Mut3_FW		AGCAGCAGCATTTCACACAAGAATAATCAGGTTC
cMet_Mut3_RV		GCTGCTGCTGCCCTTTGGACCGTCAAGAAG
cMet_Mut4_FW		AGCAGCATCCACAAAGAAGGAAGTG
cMet_Mut4_RV		GCTGCTGCTTCTGTGAGAATACACTC
cMet_Mut5_FW		GCAGCAGCAGCAGCAGCATCTGCCATGTGTGCATTC
cMet_Mut5_RV		TGCTGCTGCTGCTGCTGCTGCGAACACCCCGAAAAG
B1_Mut1_FW	Mutagenesis primers designed using NEB BaseChanger software to create point mutations in pLVX-Het1-β_1-HA, replacing specified amino acids (**Supplemental Table S1**) with alanine residues.	TGGAAATTTGGCATCTCCAGAAGGTG
B1_Mut1_RV		GATATGCGCTGTTTTCCAAC
B1_Mut2_FW		TGCCGGGTTTGCATTTGCTGGAGATGG
B1_Mut2_RV		TCTGTGGAAAACACCAGC
B1_Mut3_FW		CGGGTTTCACGCAGCTGGAGATG
B1_Mut3_RV		GCATCTGTGGAAAACACC
B1_Mut4_FW		CTTTGCTGGAGCAGGGAAACTTGG
B1_Mut4_RV		TGAAACCCGGCATCTGTG
B1_Mut5_FW		AGATGGGAAAGCAGGTGGCATTGTTTTACC
B1_Mut5_RV		CCAGCAAAGTGAAACCCG

SUPPLEMENTARY METHODS

Chamber Slides

We plated 10,000 U87 or MDA-MB-231 cells with or without the iDimerize system per well in chamber slides (Labtek by Thermo, #177402). Cells were incubated for 24 hours to allow them to adhere, after which they were treated with or without 500 nM A/C ligand for 12 hours. Following completion of PLA per protocol from main paper methods, cells were then stained with 2.5 μg/mL phalloidin (Sigma #P5282) in TNB buffer (100 mM Tris-HCl pH 7.5, 200 mM NaCl, 1% BSA) for one hour, after which the stain was washed and slides were Fluoromount-DAPI mounted.

Morphology Assessment.

Transduced MDA-MB-231 or U87 cells were plated on fibronectin coated (10 μg/mL for one hour) 8-well chamber slides and induced with 500 nM AP219667 (Takara Bio, 635055) (24 hrs). Cells were fixed with 3.7% paraformaldehyde (15 min), PBS washed, and blocked with 1% BSA (1 hr), permeabilized with 0.1% Triton-X 100 in PBS (10 min), washed three times, and incubated with Alexa488-conjugated phalloidin (Life Technologies, A12379) (30 mins). The stain was washed and slides were Fluoromount-DAPI mounted. ImageJ Form Factor plugin was used to calculate circularity shape factor (isoperimetric quotient), defined as $4X\pi X(\text{area})/(\text{perimeter})^2$ (1). The circularity shape factor of a circle is 1, and becomes much less than one for a starfish.

Survival Assays.

To assess cell survival in hypoxia and nutrient (serum) deprivation. U87-iDimerize-c-Met-β1 cells were plated on 100 mm dishes at 500K cells/dish. Cells were allowed to adhere over night. Plates were incubated in DMEM F12 high glucose media with 10% FBS for 2 hours. Media was aspirated and each plate was washed with 10mL PBS twice. Appropriate

media was added to each plate with or without FBS (for nutrient deprivation). 500 nM A/C ligand was added to complete or serum-free media for half of the dishes. Cells were incubated in normoxic or hypoxic (1% oxygen) incubators for 24 hours, then media was aspirated gently, and washed with 5 mL PBS. Light microscopy was used to image six sections of each plate at the same coordinates at 10X. De-identified images were loaded into ImageJ. Cells at 24 hours were counted per each image using the Cell Counter ImageJ plugin and averaged.

qPCR

Tissue digestion buffer was made with RPMI 1640 with 10% FBS and 10 mg/mL of both DNAse and Collagenase IV. Left lobe of the lung was severed and minced in petri dish with 300 μL of added digestion buffer. Minced lung tissue was transferred to 7 mL of digestion buffer and incubated with rotation at 37^{o}C for 40 minutes. Cell suspension was filtered through a 40 micron filter and washed once with PBS. Cells were pelleted and treated with 1X RBC lysis buffer to remove red blood cell contamination. Cells were then washed twice and pelleted down. The cell pellet was then resuspended in Buffer ATL (Qiagen) and DNA was extracted from the cells following manufacturer's protocol for DNeasy Blood and Tissue kit. DNA concentration was measured using a Take3 microspot plate and a working stock of all samples at 10 ng/μL was created to allow for identical DNA input in each reaction. Quantitative PCR was carried out using Power Syber Green Master Mix and amplified using an Applied Biosystems StepOne Real-Time PCR cycler following the recommended guidelines for Syber: 95°C for 10 minutes, followed by 40 cycles of 95°C for 15 seconds and 60°C for 1 minute. Samples were prepared with three technical replicates for each primer pair and used Actb as a control housekeeping gene. Each AC-treated sample was normalized to both Actb and its paired posit-treatment time point, with fold change calculated using the 2^(-ΔΔCt) method.

Site-directed mutagenesis

Addgene plasmid stocks were used to obtain constructs containing ITGB1 and MET (#16042 and #31786 respectively). Primers were created to amplify cMet from its vector, with hanging sequences added to attach a FLAG (DYKDDDDK) tag to the 3' end of the gene, as well as to create *NotI* digestion sites at both 5' and 3' ends. This process was repeated for β1, adding an EcoRI site to the 5' end and an HA (YPYDVPDYA) tag and XbaI sequence to the 3' end. These amplified sequences were cloned into separate pLVX-IRES-Puro empty vectors, creating pLVX-cMet-FLAG and pLVX-Beta1-HA. For β1 integrin, the Rosetta ALA scanning method (2, 3) was used to predict changes in delta-delta-G (the higher the better) when altering individual residues, with the following residues chosen to alter to alanine based on their high delta-delta-G values: ASP 226 (1.71), HIS 263 (1.76), PHE 264 (2.77), ASP 267 (3.45), and LEU 270 (2.41). For c-Met, the PyMOL model suggested that the loops atop its propeller structure make contact with β1, so we mutated these loop residues: 201-205, 241-245, 267-273, 303-307, and 348-359. All positions were converted from their original sequence to 'GCA' in order to obtain single/sequential alanine residues. Mutagenesis PCR was performed using the NEB Q5 Site Directed Mutagenesis Kit (E0554S), following manufacturer's protocol and utilizing NEB BasecChanger™ to create mutagenic primers (**Supplemental Table S4**). Mutations were confirmed by miniprep and sequencing of selected colonies before growth of larger stocks for transfection into HEK cells.

Immunofluorescence

Frozen tissue sections were stained as previously described (4). For primary antibodies, we used rabbit monoclonal anti-vimentin (1:250, Abcam, ab16700) and Alexa594 conjugated isolectin GS-IB_4 (1:250, Life Technologies, I21413). For secondary antibody, we used donkey anti-rabbit Alexa 488 (1:250, Life Technologies, A21206).

Far-Western Blotting

Lysates were first harvested into radio immunoprecipitation buffer (RIPA) containing 20mM Tris-HCl (pH 7.5), 150mM NaCl, 1mM Na_2EDTA, 1% NP-40, 1% sodium deoxycholate, 2.5mM sodium pyrophosphate, 1mM beta-glycorophosphate, 1mM Na_3VO_4, 1μg/ml leupeptin (RIPA Buffer, 10x, Cell Signaling, Technology, MA; #9806) and one tablet each of PhoStop and Complete Mini (Roche, IN). Removal of insoluble materials was achieved by centrifugation at 14,000 rpm for 20 min at 4°C. Protein concentration was then determined using the bicinchronic acid (BCA) assay (Pierce Biotechnology, Rockford, IL). Resulting lysates were electrophoresed on an SDS-PAGE gel. After transfer the PVDF blot was prepared for far-western probing as described by Wu et al. (5). Briefly, the PVDF membrane was treated with decreasing amounts of Guanidine HCl to denature and then renature the proteins within the membrane. The blots were then incubated for variable time with recombinant extracellular (SINO Biologicals; #10692-H08H-5) or intracellular c-Met (Abcam, ab42612) and then probed for the histidine repeat tag using the HisProbe™-HRP kit (Pierce Biotechnology, IL; #15165).

Dot Blotting

One μg of the following proteins were spotted onto a PVDF membrane: rh-α4-integrin (Origene Technologies, #TP314408), rh-α5-integrin (Novoprotein Scientific, #C478), rh-β1-integrin (Origene Technologies, #TP303818), and rh-c-Met (Abcam, cat. #ab42612). PVDF membranes were completely dried at room temperature before blocking with 5% non-fat dry milk. Membranes were then probed with fibronectin-GST (Kerafast, cat. #EUR108) in protein binding buffer described by Wu et al. (5) overnight at 4ºC. Resulting membranes were detected using HRP-conjugated GST antibody (Cell Signaling, #5474) using radiographic film.

Biotinylation of Cell Proteins

To biotinylate all extracellular portions, U87 cells were treated with a biotinylation kit (Life Technologies, #21115) per protocol, after which cell lysates were incubated with avidin-conjugated beads (Life Technologies) and eluted. The non-biotinylated proteins in the eluant and the biotinylated proteins bound to beads were then run on a gel and blotted with HRP-conjugated streptavidin (Perkin Elmer, #FP1047) to confirm the effectiveness of the biotinylation reaction. The non-biotinylated proteins in the eluant then underwent immunoblotting for β1 and c-Met, along with β1 and c-Met immunoprecipitation for both proteins followed by blotting of the precipitant for β1 and c-Met.

Adhesion Assay

96 well plates were coated with 20 μg/mL fibronectin overnight at 4°C. After blocking with blocking buffer (0.5% BSA in DMEM), plates were washed with washing buffer (0.1% BSA in DMEM), and then chilled. Tumor cells (50 μL at 4 X 10^5 cells/mL) were pre-incubated with varying concentrations of HGF, then added to wells and incubated for 30 minutes at 37°C. Plates were shaken at 2000 rpm for 10-15 seconds, washed 3 times in washing buffer, fixed with 4% paraformaldehyde for 10 minutes at room temperature, washed with washing buffer, stained with crystal violet for 10 minutes, washed with water, dried upside down, incubated in 2% SDS for 30 minutes at room temperature, and absorbance was read at 590 nm.

Kinase Assay

Recombinant human ILK (400 ng used with c-Met, 0, 100, 200, 300, and 400 ng used with ILK; Abcam, MA, USA; ab83119) and/or recombinant target protein (1.5 μL of 0.2 mg/mL recombinant intracellular c-Met amino acids 956-1390; Abcam ab42612 or 300 nM of unactive human AKT-1; SignalChem, cat#A16-14G). 1 μL of 10x TBS was added to each reaction,

followed by 1 μL of 50 mM of $MgCl_2$ or 100mM $MnCl_2$. Each reaction then received 1 μL of 5 mM ATPγS (Boehringer-Mannheim). Nuclease-free water was added to each reaction to bring it to a final volume of 10 μL. The reactions were then incubated at room temperature under gentle agitation for 1 hour. Each reaction was then quenched with 2.5 μL of EDTA for a total of 5 minutes. This was followed by the addition of 0.5 μL of 12 mg/mL PNBM (Abcam ab138910) to all three reactions and incubated for 45 minutes. During this time 1x loading sample was made by adding 4.3 μL of 4X LDS NuPage loading buffer to 0.7 μL of DTT stock (Cell Signaling). Loading buffer was added to each sample. The samples were then run on a standard immunoblotting assay as described below.

Drug treatment of cultured cells

OS2966 (Oncosynergy), ornatuzamab (Genentech), and NK4 (K. Matsumoto, Kringle Pharma) were kindly provided by manufacturing companies through MTAs. Cpd 22 (Calbiochem) was dissolved in DMSO. U87 cells were plated in 10 cm dishes, allowed to adhere overnight, serum starved for 2 hours, and then treated with drugs in serum-free media at concentrations and time points specified in figure legends. Lysates were then harvested for western blots and IPs.

Human Tissue Procurement and Clinical Data

Site-directed tumor biopsies were performed utilizing a 3-dimensional intraoperative navigation system. All other human tissue was obtained through the UCSF breast and brain tumor research center tissue banks, who acquired the tissue through informed consent. Patient survival data was obtained through the available clinical databases at UCSF and analyzed as described in the statistics section.

Deposited microarray analysis

We extracted archived microarray data (GEO accession number GSE79446) containing comparative genomic hybridization analysis on 8 sets of paired primary and metastatic breast tumor samples (6). That analysis was performed on paraffin-embedded tumor chunks prepped for array labelling using Agilent Oligonucleotide Array-Based CGH for Genomic DNA Analysis kit, with probes hybridized to the Human Whole Genome 8x60k chip. We downloaded the data for each sample, displayed as the log (fold change), with fold change for each gene reported as the value of the gene of interest in the sample divided by the value of the gene of interest in the reference genome. This log (fold change) value was extracted for Beta-1 (ITGB1) and c-Met (MET). All primary tumor values for each gene were converted to raw fold change and averaged to create a single primary fold change value for each of the two genes. This process was repeated for the eight metastatic tumor samples.

Statistics

For comparing continuous variables, ANOVA/t-test (parametric) or Kruskal Wallis/Wilcoxon rank sum test (non-parametric) were used, with analysis on SPSS (IBM, v24.0). Cox proportional hazards was used to identify contributions of individual variables to patient survival. Error bars are standard deviations. The threshold for statistical significance was $P<0.05$.

REFERENCES FOR SI APPENDIX

1. Levi-Schaffer F, Slovik D, Armetti L, Pickholtz D, & Touitou E (2000) Activation and inhibition of mast cells degranulation affect their morphometric parameters. *Life Sci* 66(21):PL283-290.
2. Kortemme T, Kim DE, & Baker D (2004) Computational alanine scanning of protein-protein interfaces. *Sci STKE* 2004(219):pl2.
3. Kortemme T & Baker D (2002) A simple physical model for binding energy hot spots in protein-protein complexes. *Proc Natl Acad Sci U S A* 99(22):14116-14121.
4. Carbonell WS, Delay M, Jahangiri A, Park CC, & Aghi MK (2013) beta1 Integrin Targeting Potentiates Antiangiogenic Therapy and Inhibits the Growth of Bevacizumab-Resistant Glioblastoma. *Cancer research* 73(10):3145-3154.
5. Wu Y, Li Q, & Chen XZ (2007) Detecting protein-protein interactions by Far western blotting. *Nat Protoc* 2(12):3278-3284.
6. Manso L*, et al.* (2016) Analysis of Paired Primary-Metastatic Hormone-Receptor Positive Breast Tumors (HRPBC) Uncovers Potential Novel Drivers of Hormonal Resistance. *PLoS One* 11(5):e0155840.